PERGAMON

Applied Geochemistry 15 (2000) 1265–1290

Applied Geochemistry

www.elsevier.com/locate/apgeochem

Hydrothermal alteration of felsic volcanic rocks associated with massive sulphide deposition in the northern Iberian Pyrite Belt (SW Spain)

Javier Sánchez-España*, Francisco Velasco, Iñaki Yusta

Departamento de Mineralogía y Petrología, Universidad del País Vasco, Apdo. 644, E-48080, Bilbao, Spain

Received 1 October 1998; accepted 17 November 1999
Editorial handling by R. Davy

Abstract

Massive sulphide deposits of the northern Iberian Pyrite Belt (IPB) are mainly hosted by felsic volcanic rocks of rhyolitic to dacitic composition. Beneath most of the massive ores of this area (e.g., Concepción, San Miguel, Aguas Teñidas Este or San Telmo deposits) there is usually a wide hydrothermal alteration halo associated with stockwork-type mineralization. Within these alteration envelopes there are two principal rock types: (1) chlorite-rich rocks, linked to the inner and more intensely altered zones and dominantly comprising chlorite + pyrite + quartz + sericite (+ carbonate + rutile + zircon + chalcopyrite), and (2) sericite-rich rocks, more common in the peripheral zones and showing a dominant paragenesis of sericite + quartz + pyrite + chlorite (+ carbonate + rutile + zircon + sphalerite). Mass-balance calculations comparing altered and least-altered felsic volcanic rocks suggest that sericitization was accompanied by moderate enrichment in Mg, Fe and H_2O, with depletion in Si, Na and K, and a slight net mass loss of about 3%. Chloritization shows an overall pattern which is similar to that of the sericitic alteration, but with large gains in Fe, Mg and H_2O (and minor enrichment in Si, S and Mn), and a significant loss of Na and K and a minor loss of Ca and Rb. However, chloritization has involved a much larger net mass change (mass gain of about 28%). Only a few elements such as Nb, Y, Zr, Ti, P and LREE appear to have remained inert during hydrothermal alteration, whilst Ti and Al have undergone very minor mobilization. The results point to the severity of the physico-chemical conditions that prevailed during the waxing stage of the ore-forming hydrothermal systems. Further, mineralogical and geochemical studies of the altered footwall rocks in the studied deposits indicate that hydrothermal ore-bearing fluids reacted with host rocks in a multi-stage process which produced a succession of mineralogical and chemical changes as the temperature increased.

1. Introduction

Hydrothermal alteration affecting the host rocks of massive sulphide deposits has been widely studied and extensively documented. Excellent examples on this subject are shown by Canadian volcanic-hosted massive sulphide (VHMS) deposits (Franklin et al., 1981; Gibson et al., 1983; Urabe and Scott, 1983; Lesher et al., 1986; MacLean and Barrett, 1993; Barrett and MacLean,1994; Lentz and Goodfellow, 1993, 1996),

* Corresponding author. Fax: +34-4-464-85-00.
E-mail address: npbsaesj@lg.ehu.es (J. Sánchez-España).

0883-2927/00/$ - see front matter
PII: S0883-2927(99)00119-5

Australian VHMS deposits (Large, 1977, 1992; Gemmell and Large, 1992; Huston, 1993) and Kuroko-type mineralization in Japan (Bryndzia et al., 1983; Pisutha-Arnold and Ohmoto, 1983; Urabe et al., 1983; Ohmoto, 1996). Other studies include present-day hydrothermal systems on the modern sea floor (Seyfried et al., 1988; Goodfellow and Peter, 1994). From this research it is generally accepted that the hydrothermal alteration envelopes that surround the footwall rocks beneath the massive sulphides have developed as a consequence of intense interaction between hot hydrothermal ore-bearing fluids (convectively-circulating evolved sea water) and the wall rocks. This process occurred contemporaneously with the formation of the massive sulphides on the ocean floor. Subsequent chemical and isotopic changes in the rocks are due to metasomatism in an open system, in response to variations of physico-chemical factors such as temperature, O_2 and S_2 fugacities or water/rock ratio.

Similar zones of hydrothermal alteration have been found in association with most massive sulphide deposits of the Iberian Pyrite Belt (IPB). These zones usually have the form of wide haloes or envelopes that surround the cross-cutting stockworks which underly the massive ores. Good examples are those of Rio Tinto (García Palomero, 1980; Leistel et al., 1994), Aznalcóllar (Almodóvar et al., 1998), La Zarza (Strauss et al., 1981), and Masa Valverde (Toscano et al., 1993, 1994) in the Spanish part of the IPB, and Aljustrel (Barriga, 1983; Barriga and Fyfe, 1998) and Salgadinho (Plimer and Carvalho, 1982) in Portugal. These studies describe mineralogical changes and variable mobility of some major and trace elements in the altered host rocks of the massive sulphides. Basically, the most generalized feature appears to be an Fe–Mg enrichment and an Na–K depletion, in the proximity of the orebodies. Hydrothermal dispersion haloes with anomalous concentrations of elements, such as As, Tl, Ba, Sb or F, have been described by several authors (Schütz et al., 1988; Leistel et al., 1994). Other researchers (Strauss et al., 1981; Almodóvar et al., 1998) have proposed that the Co/Ni ratio in whole rock compositions can be used as an indicator of the degree of alteration, and Toscano et al. (1993, 1994) and Leistel et al. (1994) have outlined the advantage of using the Fe/(Fe + Mg) ratio in chlorites, or the (Ba + K)/Na value in muscovites, as potential tools in massive sulphide exploration.

Despite this knowledge of the hydrothermal alteration associated with the IPB deposits, some aspects still remain uncertain. These include the net mass changes which have occurred in altered rocks during alteration, the behavior of some high field strength (HFS) elements such as Al, Ti, Zr, Nb, Y and LREE, traditionally considered as "immobile" in most hydrothermal systems, but apparently mobile in the alteration haloes of some deposits (Pascual et al., 1997; Almodóvar et al., 1998), and finally, the chemical effects of the later Hercynian metamorphism on the altered rocks. Further, a strong contrast exists between the abundant information available for the most famous deposits (Riotinto, Aljustrel, Aznalcóllar) and the lack of data for other areas in the IPB, such as the one selected in this study.

This paper deals with the main mineral and chemical transformations undergone during hydrothermal alteration in the footwall rocks of some of the larger massive sulphide deposits (namely Concepción, San Miguel, Cueva de la Mora, Aguas Teñidas Este and San Telmo) of the northern region of the Iberian Pyrite Belt. In this work the authors describe the main petrographic and chemical features of the major mineral phases of these rocks. Chemical comparisons between altered and least-altered volcanic rocks have been made, with mass balance calculations on the basis of whole-rock geochemistry. Finally, based on the petrological and geochemical findings, the authors speculate on the likely mechanism causing the alteration of these volcanic rocks during the ore-forming hydrothermal events.

2. Geological framework

2.1. Regional geology

The IPB forms a belt 230 km long and about 40 km wide in the southwestern corner of the Iberian Peninsula, extending from the north of Sevilla in Spain, to the south of Lisboa, in Portugal (Fig. 1). The total resources of massive sulphide (exceeding 1700 million tons; Leistel et al., 1998) as well as the enormous size of many of its deposits (e.g., Riotinto or Neves-Corvo, with tonnages of about 335 and 220 million tons, respectively), make the IPB the largest concentration of massive sulphide in the world (Sáez et al., 1996; Leistel et al., 1998).

The IPB sedimentary record has been traditionally considered as comprising three main lithostratigraphic units (Schermerhorn, 1971; Fig. 2), which from older to younger are: (i) the Phyllite–Quartzite Group (PQ), composed of Upper Devonian slates, quartzites and litharenites; (ii) the Volcano-Sedimentary Complex (VSC), Lower Tournaisian to Middle Visean in age, comprising rocks of three felsic (dacitic to rhyolitic) volcanic episodes alternating with mafic volcanic and sedimentary rocks, and hosting the massive sulphides; and (iii) the Culm Group, composed of a flysch-like sequence of slates and sandstones of Upper Visean to Lower Westphalian age. All these rocks were subsequently folded and metamorphosed under low grade conditions (ranging from zeolite to lower greenschist

facies) during the Hercynian orogeny (Schermerhorn, 1971; Silva et al., 1990).

2.2. Deposit geology

The deposits studied — Concepción (CO), San Miguel (SM), Cueva de la Mora (CM), Aguas Teñidas Este (ATE) and San Telmo (ST) — are located in the northeastern corner of the IPB (Fig. 1), north of the mining districts of Riotinto and La Zarza, and form part of an E–W-trending deposit alignment. From a structural viewpoint, this area is characterized by the

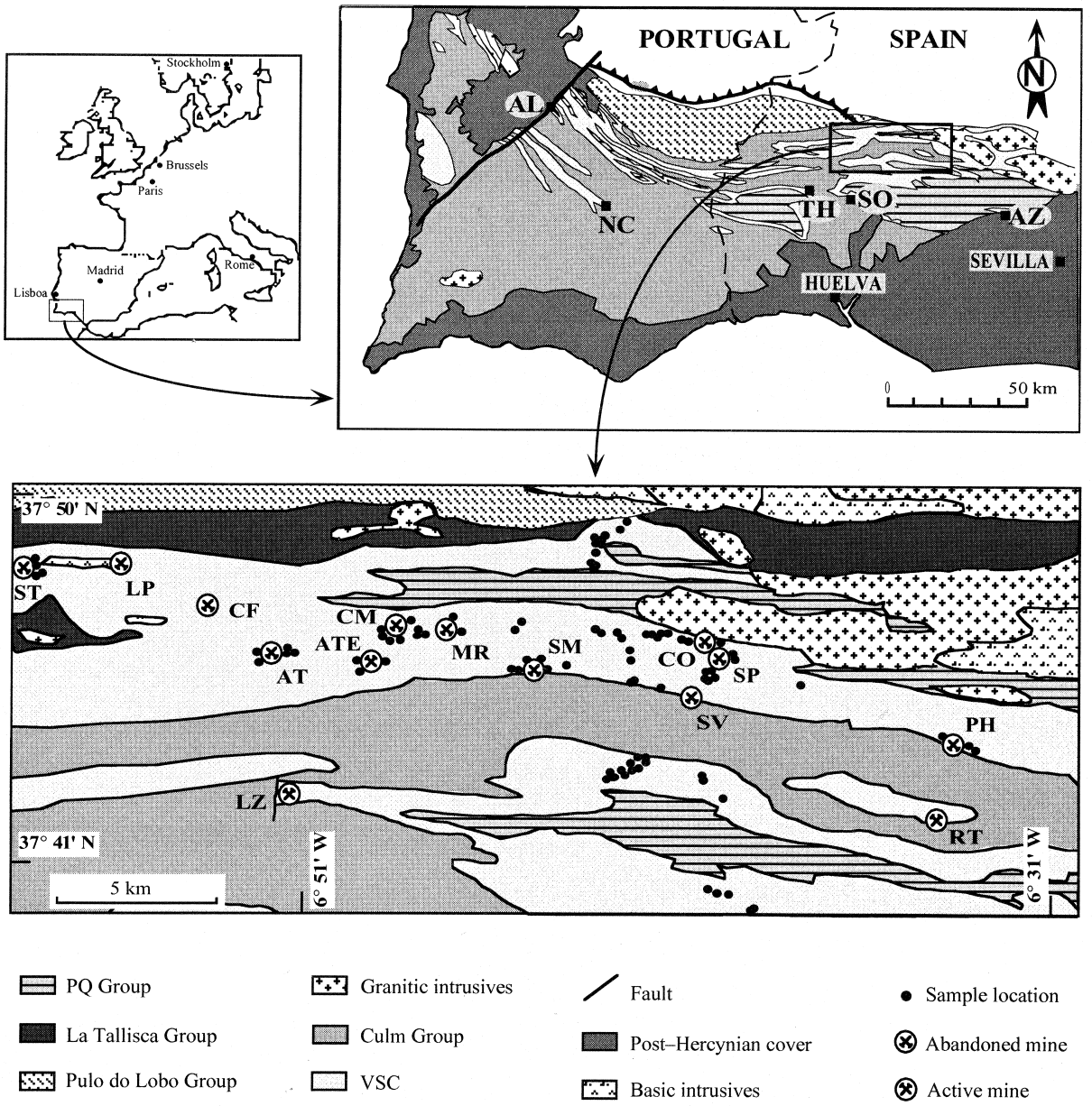

Fig. 1. Location map and simplified regional geology of the studied zone (modified from Carvalho et al., 1976; Ramírez and Navarro, 1982; Bonaño et al., 1984). Ore deposit abbreviations: AL, Aljustrel; AT, Aguas Teñidas (old mine); ATE, Aguas Teñidas Este; AZ, Aznalcóllar; CF, Confesionarios; CM, Cueva de la Mora; CO, Concepción; LP, Lomero-Poyatos; LZ, La Zarza; MR, Monte Romero; NC, Neves-Corvo; PH, Peña del Hierro; RT, Riotinto; SM, San Miguel; SO, Sotiel; SP, San Platón; ST, San Telmo; SV, Soloviejo (Mn mineralization); TH, Tharsis.

ubiquitous presence of Hercynian megastructures, including major folds of E–W orientation.

The orebody of Aguas Teñidas Este was discovered in 1983 and is being developed by Navan Resources (Huelva) S.A. (Rodríguez, 1996), whereas Concepción (whose total reserves have been recently increased after a new and successful geophysical exploration program, followed by drilling) is now under economic re-evaluation. Although relatively small when compared with the enormous deposit of Riotinto, both Aguas Teñidas Este (with total resources of 35 Mt, 1.3% Cu, 0.9% Pb, 3.1% Zn, 37 g/t Ag and 0.5 g/t Au; Rodríguez, 1996) and Concepción (in excess of 55 Mt of massive ore with 0.57% Cu, 0.19% Pb, 0.48% Zn, 6 g/t Ag and 0.2 g/t Au) are within the "very large" type of those recorded by Fernández Álvarez (1974) for the IPB deposits. San Miguel, San Telmo and Cueva de la Mora are presently out of production. Their original reserves of massive ore were 1.3 Mt (3% Cu), 4.0 Mt (1.2% Cu, 0.4% Pb, 12% Zn, 60 g/t Ag and 0.8 g/t Au) and 4.2 Mt (1.45% Cu, 0.3% Pb and 0.73% Zn), respectively (Pinedo Vara, 1963).

Most of the deposits are hosted by felsic volcanic rocks at the top of the V_{A1} and V_{A2} felsic volcanic episodes (Fig. 2), although some are locally interbedded, or associated with, fine-grained tuffites and/or shales (Figs. 2–5; Lécolle, 1977; Mitsuno et al., 1988; Sáez et al., 1996). Host rocks include felsic lava and breccias, but most commonly consist of pyroclastic rocks (mainly, porphyritic crystal-lithic lapilli tuffs), ranging from high-SiO_2 rhyolite to dacite in composition (Sánchez-España et al., 1997). These rocks have been interpreted in the general context of the IPB as products of explosive volcanism of acid calc-alkaline magmas in a shallow marine environment (Routhier et al., 1978; Barriga, 1983; Thiéblemont et al., 1994; Sáez et al., 1996; Leistel et al., 1998). However, some authors have proposed a subvolcanic character as peperitic sills injected into wet sediments (Boulter, 1993a, b; Mitjavilla et al., 1997). It has been suggested that the felsic magmas were derived from partial melting (caused by ascending tholeiitic magmas) of a greywacke-type continental source in a spreading back-arc environment, during Dinantian times (Munhá, 1983; Thiéblemont et al., 1994; Sáez et al., 1996; Mitjavilla et al., 1997; Leistel et al., 1998).

The orebodies are usually tabular to lenticular in shape, with the mineralization mainly composed of pyrite, with variable but lesser amounts of sphalerite, chalcopyrite and galena. Other minor minerals are tetrahedrite–tennantite, arsenopyrite, magnetite, pyrrhotite, cassiterite and hematite. Gangue minerals include quartz, chlorite, sericite, carbonate and rare barite.

Most deposits usually exhibit a well-developed stockwork below the massive mineralization (e.g., Aguas Teñidas Este, San Miguel and Concepción;

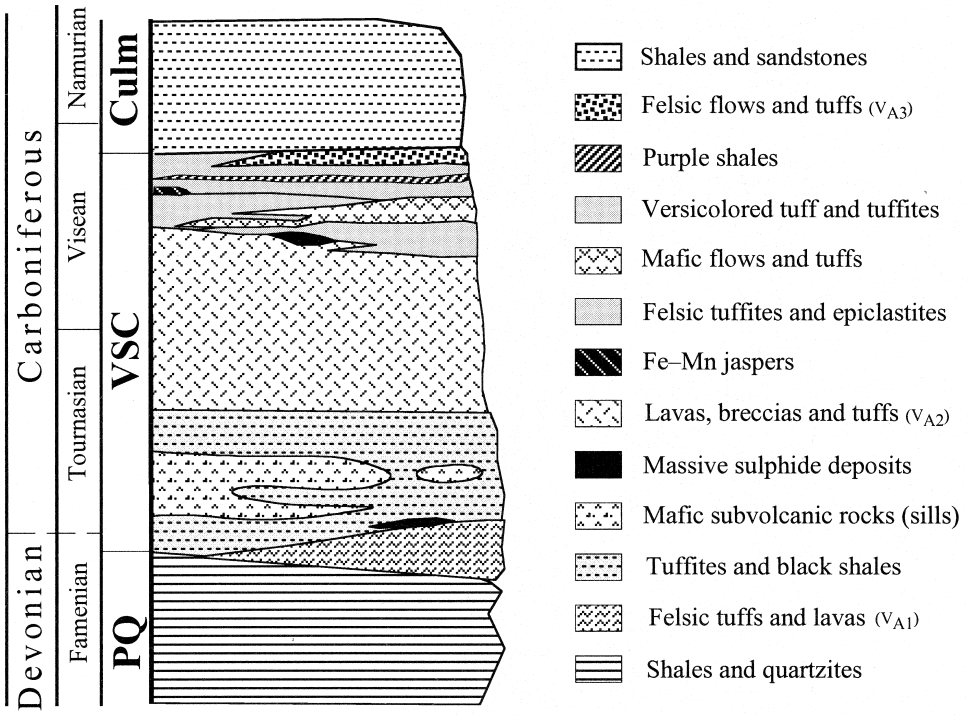

Fig. 2. Simplified stratigraphic sequence for the studied zone (modified from Sáez et al., 1996).

Figs. 4 and 5), with similar characteristics to those described in many other massive sulphide districts (e.g., Lydon, 1988a; Large, 1992). In the periphery of these stockworks, wall rocks are affected by intense hydrothermal alteration, which obliterates any previous volcanic fabric, transforming them to chloritic and/or quartz–sericitic rocks. Other alteration minerals such as carbonate and sulphide have been recognized in some deposits, especially in the footwalls proximal to the massive ores.

As in many other classical examples of VHMS deposits throughout the world, a clear chemical zoning can be recognized in many IPB deposits: the massive ores are often Cu-rich in the stockworks and at the base of the sulphide horizons, and Zn–Pb–Ag-rich in the upper zones (e.g., Concepción; Fig. 3). The alteration haloes surrounding the stockworks commonly have an inner chloritic core, surrounded by a sericitic peripheral zone (e.g., Aguas Teñidas Este; Fig. 5).

A recent study carried out on the IPB deposits has shown a correlation between their $\delta^{34}S$ signatures and textural evolution (Velasco et al., 1998). These authors noted that the Northern IPB deposits show textures characteristic of hydrothermal replacement and recrystallization, and have higher $\delta^{34}S$ values (+2.5 to +10.1‰) than those situated in the Southern IPB (e.g., Tharsis, Sotiel or Aznalcóllar; see Fig. 1), which show a predominance of primary textures and lighter S ($\delta^{34}S = -26.5$ to +5.6‰). The reported data suggest a bacteriogenic origin for the S in the primary fine-grained ores, whereas the coarse-grained sulphides and the stockwork veins (e.g., Concepción, with $\delta^{34}S = 8$–10‰) indicate the prevalence of hydrothermal H_2S, which was probably produced by inorganic reduction of contemporaneous seawater SO_4 (Velasco et al., 1998).

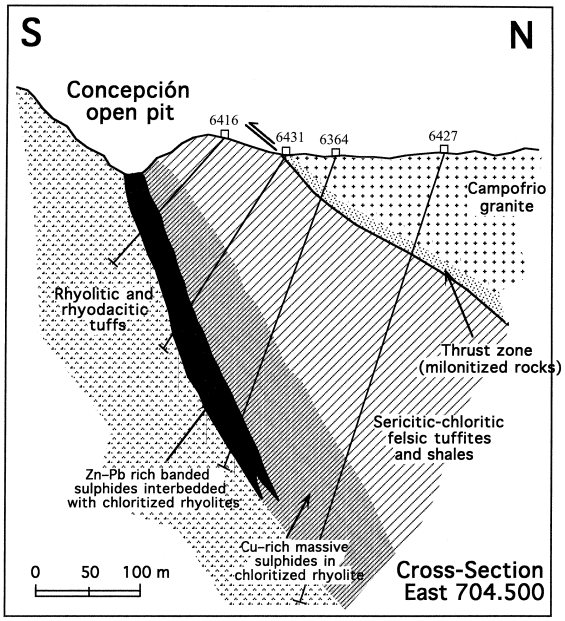

Fig. 3. Schematic cross-section of the Concepción deposit (after Rio Tinto Minera S.A., 1993, unpublished). Massive sulphides are interbedded with intensely chloritized felsic pyroclastics, and comprise from true footwall to hangingwall: (i) pyrite dissemination and stockwork-type mineralization in chloritized felsic pyroclastic rock; (ii) massive pyrite–chalcopyrite ore with thin magnetite layers; and (iii) the uppermost fine-grained banded pyrite–sphalerite–galena ore. Approximate location and numbers of some drill-holes are also shown.

3. Methodology and analytical procedures

One hundred and seventy six samples were collected. Thirty four samples came from drillcores, with 92 samples from open pits and 50 from outcrops. These samples included hydrothermally-altered rocks from the footwall regions of the ore deposits, and least-altered rocks (mainly rhyolitic dacitic volcanics, but also comprising more intermediate to basic rocks, tuffites and shales) collected from areas distal to the deposits. The samples ($\approx$1 kg weight) were cleaned to remove weathered surfaces, crushed, and then ground in a tungsten carbide disc mill, in order to obtain a fine rock dust of less than 240 mesh (<63 μm in diameter). Analyses were made on sample powders, fused with an Li-borate flux, as well as on pressed powder pellets, following the method described in Yusta et al. (1994). Ten major and 25 trace elements were determined by wavelength dispersive X-ray fluorescence, using an automated Philips PW 1480 spectrometer at the Laboratorio de Mineralogía de la Universidad del País Vasco (Bilbao, Spain). Polished thin sections of the analysed rocks were studied under transmitted and reflected light microscopes to identify the mineral assemblages of both altered and least-altered rocks. Chemical analyses of the major minerals were performed using a Cameca SX-50 electronic microprobe at the Laboratoire de Minéralogie de l'Université Paul Sabatier (Toulouse, France). Microthermometric measurements of fluid inclusions were determined at the Universidad del País Vasco, after detailed petrographic examination, in $\approx$200 μm-thick doubly-polished wafers of 20 samples of stockwork vein quartz from the Aguas Teñidas Este, San Miguel and San Telmo deposits, using a modified Chaixmeca heating–freezing stage with a high power (ULWD ×80, Olympus) objective lens.

Several data-processing and statistical techniques have been used to characterize the geochemical features of hydrothermal alteration. For determining mass changes related to hydrothermal alteration pro-

cesses, the isocon method has been used. This method was initially developed by Grant (1986) after Gresens (1967) equations. Specifically, a later version developed by Baumgartner and Olsen (1995), which introduced a computational routine in FORTRAN, with a least-squares approach for the isocon calculations, was used. The "Gresens' 92" application of Potdevin (1993) has also been applied for the mass change estimations.

4. Results

4.1. Alteration types

Four main alteration episodes dating from Late Devonian to recent times have been recognized in the studied deposits:

1. Regional alteration occurred in association with the Upper Devonian volcanism, transforming the original basalts into spilites and the felsic rocks (dacites and rhyolites) into keratophyres and/or quartz–keratophyres. This so-called "*hydrothermal metamorphism*" (Munhá and Kerrich, 1980) has been considered to be the result of an intense interaction between seawater and the volcanic rocks, soon after the extrusion of the latter. Although some authors have suggested these rocks are of primary magmatic origin (Schermerhorn, 1970; Soler, 1973), other workers (Munhá and Kerrich, 1980; Munhá, 1990; Sáez et al., 1996) point to post-magmatic metasomatic processes (e.g., albitization, sericitization and/or chloritization) to explain their formation.
2. A more focused and intense hydrothermal alteration, linked to the footwall and stockwork zones beneath the massive sulphides, occurred during sulphide deposition. In this case, an intense metasomatism took place between the volcanic rocks and hot ore-bearing hydrothermal fluids, contemporaneous with the sulphide deposition. As discussed below, this alteration is responsible for the main textural and chemical transformations observed in the studied rocks, and is the main subject of this study.

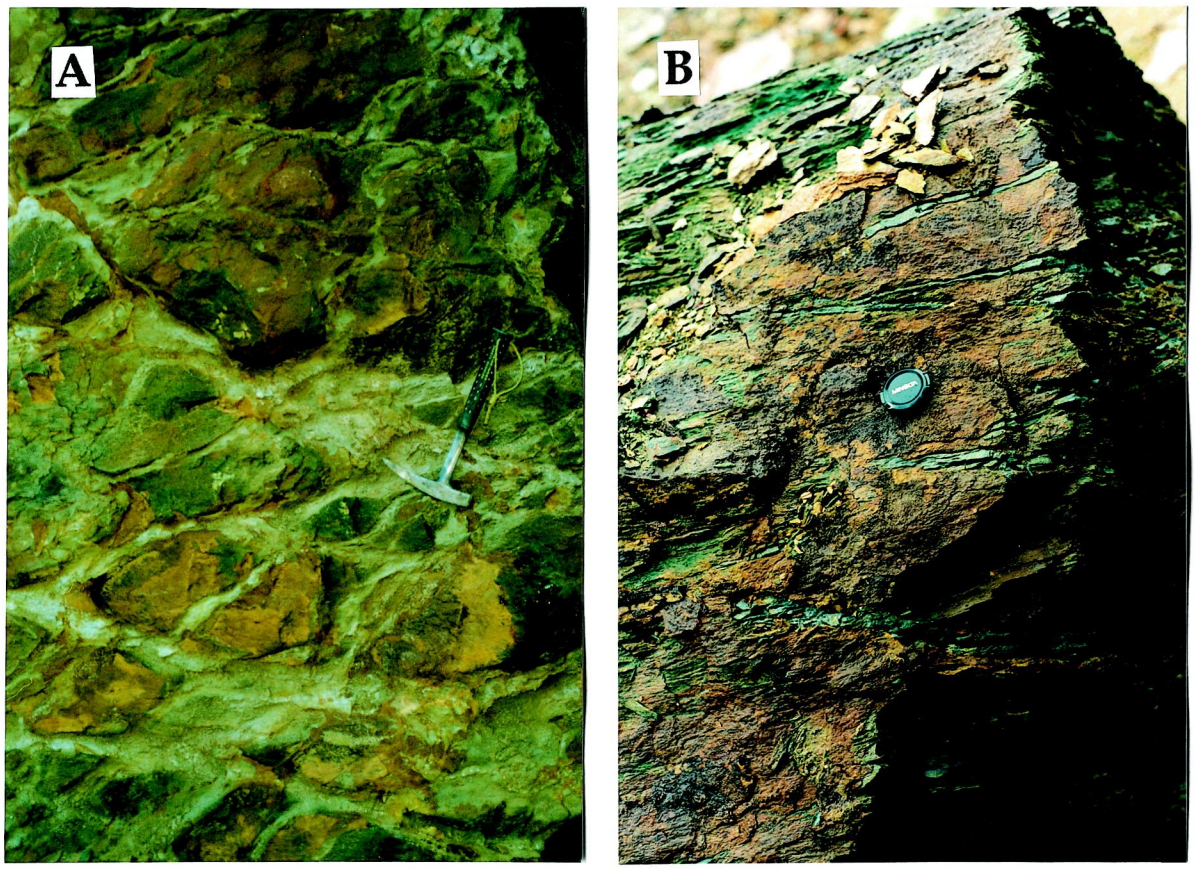

Fig. 4. (A) Partial view of San Miguel stockwork, developed in intensely altered rhyolite. (B) Detail of Concepción stockwork, showing the anastomosing quartz–sulphide veins in chloritized rhyolite (sample not in situ).

3. A low to very low-grade regional metamorphism, which took place during Hercynian times. This episode does not seem to have affected the previous rock mineralogy, and only some recrystallization should be attributed to this event. Although the intensity of both metamorphism and deformation has been traditionally considered to increase from SW to NE across the IPB (Lécolle, 1977; Routier et al., 1978; Munhá, 1979, 1990), recent studies (Fernández-Caliani et al., 1994; Sáez et al., 1996; Sánchez-España and Velasco, 1999) have documented the lack of such regional zoning, suggesting the possibility of a regional metamorphism focused along shear zones.
4. Finally, supergene alteration with some rocks affected by intense weathering due to exposure to mine and meteoric waters. This latter process (which is clearly visible in the vicinity of the mines) has produced its own mineralogical and chemical transformations (e.g., oxidation of the primary minerals with formation of hematite and/or goethite, precipitation of Cu and Fe–sulphate, etc.); all rocks showing supergene alteration have been avoided in this study.

4.2. Alteration petrography

Distal to the alteration zones, least-altered felsic volcanic rocks are composed of medium-grained (0.5–2 mm) euhedral quartz and feldspar phenocrysts in a fine-grained (micro- to cryptocrystalline) matrix, comprising quartz, feldspar, sericite, chlorite and some devitrified glass (Fig. 6(A)). Accessory minerals include epidote, calcite, chloritized biotite,

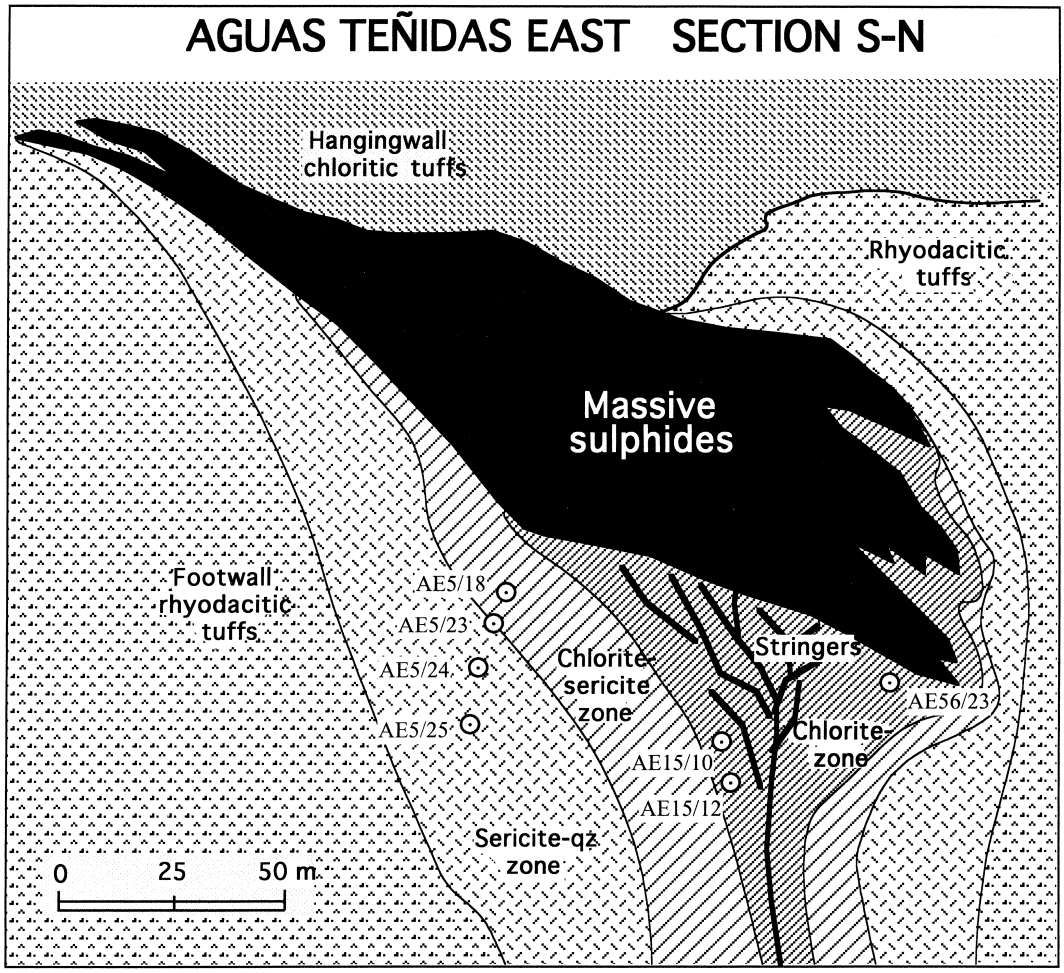

Fig. 5. Schematic cross-section of the Aguas Teñidas Este (ATE) massive sulphide orebody and associated stockwork, showing the footwall hydrothermal alteration envelope (modified from Bobrowicz, 1995; Rodríguez, 1996).

zircon and hematite. Feldspars are apparently little altered, being fresh or weakly sericitized. Albite is the most common feldspar, being present either as phenocrysts (with abundant antiperthitic and myrmekitic textures) or as fine-grained microlites in the matrix. Some K-feldspar has also been observed with albite in the least-altered rocks. Although the K-feldspar is more common in the groundmass, some is present as rare phenocrysts and/or finely intergrown with quartz, forming spherulitic and granophyric textures. Textural evidence exists for the replacement of early (primary) alkali feldspar by albite of secondary origin, which appears to have occurred during the earliest regional hydrothermal alteration.

In the stockwork zones underlying the massive sulphides, intense hydrothermal alteration has transformed the least-altered rocks, which now exhibit a dominant paragenesis of chlorite + quartz + sericite + pyrite (+ carbonate + rutile + zircon + chalcopyrite) in the inner and more intensely altered zones, and sericite + quartz + pyrite + chlorite (+ carbonate + sphalerite + rutile + zircon) in more peripheral areas. These assemblages are very similar to those found in the footwall alteration zones of other IPB deposits, such as Rio Tinto (García Palomero, 1980; Leistel et al., 1994), Aljustrel (Barriga, 1983; Barriga and Fyfe, 1998), Aznalcóllar (Almodóvar et al., 1998), Tharsis (Tornos et al., 1998) and Masa Valverde (Toscano et al., 1993).

The altered rocks reveal clear signs of secondary mineral formation:

1. In sericitized rocks, feldspars are usually transformed into sericite, quartz–sericite or coarse-

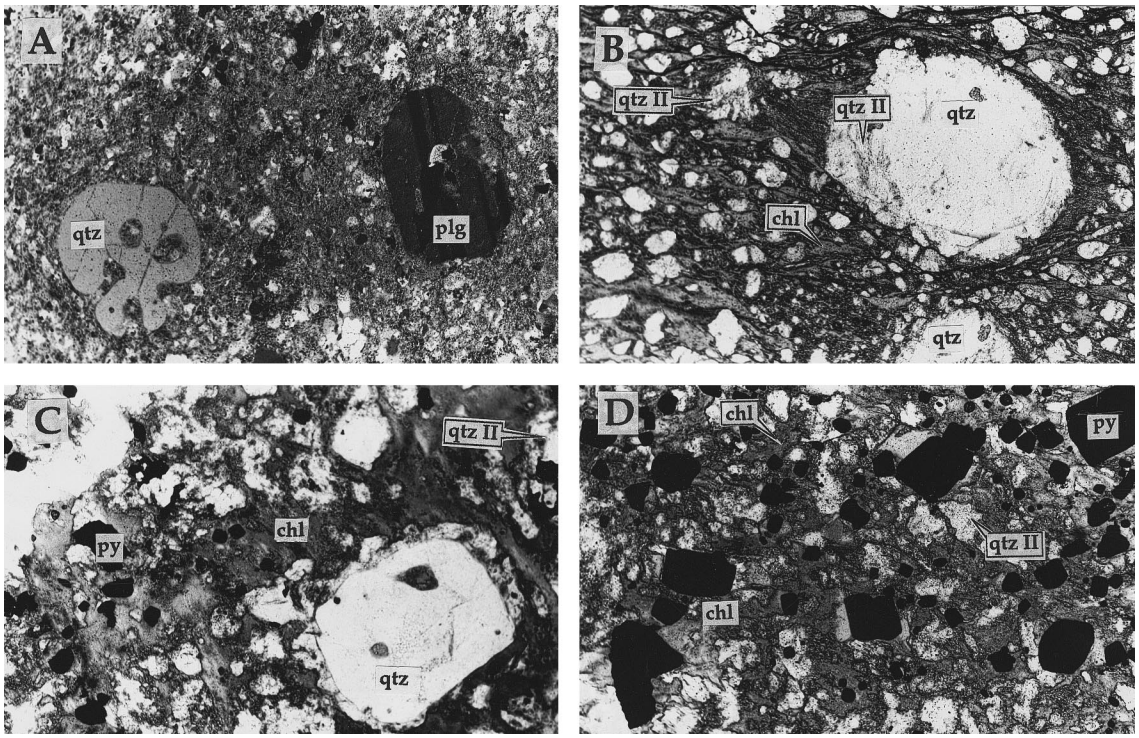

Fig. 6. Transmitted-light photomicrographs of some least-altered to intensely altered volcanic rocks from the northern area of the IPB. (A) Detail of a least-altered rhyolitic lava, showing a typical porphyritic texture, with subautomorphic quartz (*qtz*) and albitic plagioclase (*plg*) phenocrysts, partly corroded and surrounded by a microcrystalline groundmass (composed of fine-grained quartz, plagioclase, sericite, some chlorite and opaque minerals); polarized light; Odiel river outcrops. (B) Chloritized rhyolite from the Concepción stockwork; a subautomorphic volcanic quartz crystal is surrounded by a rim of secondary quartz (*qtz II*); plastic deformation of the schistose matrix (composed of fine-grained ripidolitic chlorite (*chl*) and slightly orientated fine-grained quartz crystals) has formed a pressure shadow around the phenocryst. (C) Intensely chloritized and silicified rhyolite from the ATE stockwork. Massive chlorite invades most intercrystalline spaces and surrounds unaltered (or little altered) volcanic quartz phenocrysts. Some silicification quartz and some pyrite (*Py*) can also be observed. (D) Severe alteration in San Miguel's stockwork rhyolite; in this case, intense chloritization, silicification and sulphidization have destroyed and obliterated most previous textures. Euhedral pyrite crystals are very abundant and often surrounded by secondary quartz selvages and/or chlorite. The field of view is 2 mm across in all photographs.

Table 1
Electron microprobe analyses and calculated structural formulae of some selected chlorites, white micas and feldspars from the studied rocks[a]

	Chlorites (36 oxygens)										Muscovites (24 oxygens)						Feldspar (32 oxygens)			
Sample	CO-1	CO-2	CO-3	CO-4	AE15/10	AE15/11	AE15/12	AE5/6	SM-Stk	CM-2	Sample	CO-1	CO-2	CO-3	SM-Stk	CM-23	Sample	SM-Stk	CO-2	AE56/21
Rock type	Chl	Chl	Chl	Ser	Chl	Chl	Chl	Chl	Chl	Chl	Rock type	Chl	Chl	Chl	Chl	Ser	Rock type	Chl	Chl	Chl
n	7	3	13	3	11	8	7	11	9	9	*n*	6	6	6	4	11	*n*	3	3	6
Oxide (wt.%)											Oxide (wt.%)						Oxide (wt.%)			
SiO_2	25.99	32.80	26.78	25.19	29.20	30.69	24.30	25.75	27.24	24.22	SiO_2	47.23	45.15	47.20	44.89	48.41	SiO_2	67.36	70.68	66.95
TiO_2	0.01	0.01	0.00	0.06	0.00	0.00	0.00	0.00	0.00	0.00	TiO_2	0.01	0.04	0.00	0.00	0.03	TiO_2	0.00	0.00	0.00
Al_2O_3	20.71	23.12	19.17	21.18	22.86	20.72	19.96	19.12	21.20	20.24	Al_2O_3	28.74	33.11	32.07	33.75	27.19	Al_2O_3	20.15	18.85	19.97
FeOt	23.90	14.46	28.33	24.74	4.09	3.90	28.65	26.24	17.19	30.70	FeO	3.01	1.08	1.50	1.31	3.30	FeO	0.00	0.11	0.14
MnO	0.21	0.13	0.17	0.14	0.10	0.06	0.28	0.24	0.21	0.31	MnO	0.01	0.04	0.05	0.07	0.14	MnO	0.00	0.00	0.00
MgO	14.47	16.93	11.19	14.65	29.43	30.63	12.74	15.19	18.88	10.05	MgO	2.98	1.47	1.72	3.25	3.82	MgO	0.00	0.04	0.02
CaO	0.07	0.20	0.02	0.03	0.00	0.02	0.02	0.01	0.05	0.03	CaO	0.04	0.04	0.06	0.08	0.03	CaO	0.57	0.12	0.71
Na_2O	0.00	0.15	0.02	0.03	0.68	0.03	0.05	0.13	0.08	0.01	Na_2O	0.19	0.39	0.44	1.92	0.18	Na_2O	11.97	10.69	11.69
K_2O	0.08	1.45	0.06	0.06	0.00	0.01	0.01	0.01	0.03	0.05	K_2O	9.96	9.92	9.72	9.53	10.19	K_2O	0.09	0.09	0.04
BaO	0.00	0.00	0.00	0.00	0.00	0.00	0.00	0.00	0.00	0.00	BaO	0.08	0.14	0.09	0.17	0.14	BaO	0.09	0.01	0.00
H_2O^+	11.03	12.30	10.95	11.05	12.28	12.21	10.76	10.99	11.60	10.63	H_2O^+	4.12	4.08	4.35	4.09	4.15	H_2O^+	–	–	–
F	0.26	0.25	0.20	0.20	0.64	0.85	0.30	0.45	0.24	0.20	F	0.42	0.45	0.18	0.65	0.44	F	–	–	–
—O═F	0.11	0.11	0.08	0.08	0.27	0.36	0.13	0.19	0.10	0.08	—O═F	0.18	0.19	0.08	0.27	0.19	—O═F	–	–	–
Total	96.62	101.69	96.81	97.25	99.01	98.76	96.94	97.94	96.62	96.36	Total	96.53	95.58	97.21	99.27	97.69	Total	100.23	100.59	99.52
Structural formulae											Structural formulae						Structural formulae			
Si	5.58	6.33	5.85	5.40	5.57	5.84	5.35	5.53	5.64	5.41	Si	6.54	6.26	6.42	6.05	6.65	Si	11.80	12.20	11.81
Al^{iv}	2.42	1.67	2.15	2.60	2.43	2.16	2.65	2.47	2.36	2.59	Al^{iv}	1.46	1.74	1.58	1.95	1.35	Al^{iv}	4.16	3.84	4.15
Al^{vi}	2.82	3.58	2.78	2.76	2.70	2.49	2.53	2.37	2.81	2.75	Al^{vi}	3.24	3.67	3.56	3.41	3.05	Mg	0.00	0.01	0.01
Fe^{2+}	4.29	2.33	5.17	4.44	0.65	0.62	5.27	4.71	2.98	5.74	Fe^{2+}	0.35	0.13	0.17	0.15	0.38	Ca	0.11	0.02	0.13
Mn	0.04	0.02	0.03	0.03	0.02	0.01	0.05	0.04	0.04	0.06	Mn	0.00	0.00	0.01	0.01	0.02	Na	4.07	3.58	4.00
Mg	4.63	4.87	3.64	4.68	8.36	8.69	4.18	4.86	5.82	3.35	Mg	0.62	0.30	0.35	0.65	0.78				
Ca	0.02	0.04	0.00	0.01	0.00	0.00	0.00	0.00	0.01	0.01	Ca	0.01	0.01	0.01	0.01	0.00	Mol %Or=	0.48	0.55	0.22
Na	0.00	0.06	0.01	0.01	0.25	0.01	0.02	0.05	0.03	0.00	Na	0.05	0.10	0.12	0.50	0.05	Mol %Ab=	96.97	98.84	96.54
K	0.02	0.36	0.02	0.02	0.00	0.00	0.00	0.00	0.01	0.01	K	1.76	1.75	1.69	1.64	1.79	Mol %An=	2.56	0.61	3.24
Ba	0.00	0.00	0.00	0.00	0.00	0.00	0.00	0.00	0.00	0.00	Ba	0.00	0.01	0.01	0.01	0.01				
F	0.18	0.15	0.14	0.14	0.39	0.51	0.21	0.31	0.16	0.14	F	0.18	0.20	0.08	0.28	0.19				
OH	15.81	15.84	15.96	15.82	15.63	15.52	15.81	15.76	16.03	15.87	OH	3.81	3.78	3.95	3.68	3.80				

[a] Major oxides as weight percent; *n* = number of analyses; H_2O^+, calculated water content in formula, FeOt, total iron as FeO —O═F, calculated oxygen equivalent for fluorine. Chl, Chloritized rock; Ser, Sericitized rock. Sample captions: CO, Concepción; SM, San Miguel; AE, Aguas Teñidas Este; CM, Cueva de la Mora.

grained muscovite. However, it is sometimes possible to distinguish their original tabular habits as "ghosts" in the fine-grained sericitic matrix. Quartz is better preserved, either as phenocrysts or as fine-grained crystals in the sericitic-chloritic groundmass, and it can be seen with a fibrous elongate habit in the pressure shadows surrounding some euhedral pyrite. Open spaces may be infilled with coarse-grained ankerite, calcite or quartz.

2. In chloritized rocks many quartz crystals are corroded by fine-grained massive chlorite, which also occupies intercrystalline spaces. Chlorite replaces most of the original rock matrix, and gives a strongly schistose fabric to the rock (Fig. 6(B) and (C)). Feldspar and other silicates (such as biotite) are, in most cases, totally transformed and replaced by chlorite, and the rocks grade from moderately chloritized (20–30% volume percent chlorite) to almost monomineralic chlorite (>90%) with lesser quartz, pyrite and trace sericite (Fig. 6(D)). However, the presence of feldspar ghosts and large euhedral quartz eyes in the altered rocks (which are similar to those found in the least-altered samples) support the hypothesis that these rocks are the altered equivalent of the relatively unaltered rhyolitic tuffs and lavas, found at some distance from the deposits. Carbonate, chalcopyrite, rutile and zircon are common accessory constituents. Zircon crystals included in massive chlorite are often surrounded by pleochroic metamict haloes, as noted in other IPB deposits (Pascual et al., 1997; Almodóvar et al., 1998). Other sulphides such as arsenopyrite, tetrahedrite and/or pyrrhotite (pyrrhotite as very fine inclusions within pyrite) can be present.
3. Silicification is a common process in some samples, and involves replacement of both phenocrysts (quartz and feldspar) and matrix by fine-grained granoblastic quartz. Such quartz can also form rims around phenocrysts and rock fragments. This process has transformed some of the original rhyolites into highly siliceous rocks, with more than 70% by volume of quartz. Two stages of silicification can be distinguished: an early silicification, predating both sericitization and chloritization; and a late deposition where quartz, commonly associated with pyrite and chlorite, fills veins in the central parts of the stockworks.

4.3. Mineral chemistry

Coarse feldspar in altered rocks is usually of tabular automorphic habit, single or multiply-twinned, and severely sericitized, chloritized or silicified. Microprobe data have confirmed the albitic character of these feldspars, with the average composition approaching $An_{3.00}$ (Table 1).

Sericite present in the groundmass consists of fine-grained celadonitic muscovite (Fig. 7), with phengite content (atomic Fe + Mg per formula) ranging from 0.80 to 1.15. These values are considerably higher than the mean value of 0.50, shown by coarse-grained muscovite associated with the massive ores. The Fe/(Fe + Mg) ratio of the sericite ranges from 0.10 to 0.40, and the Ba content is invariably low, with values of

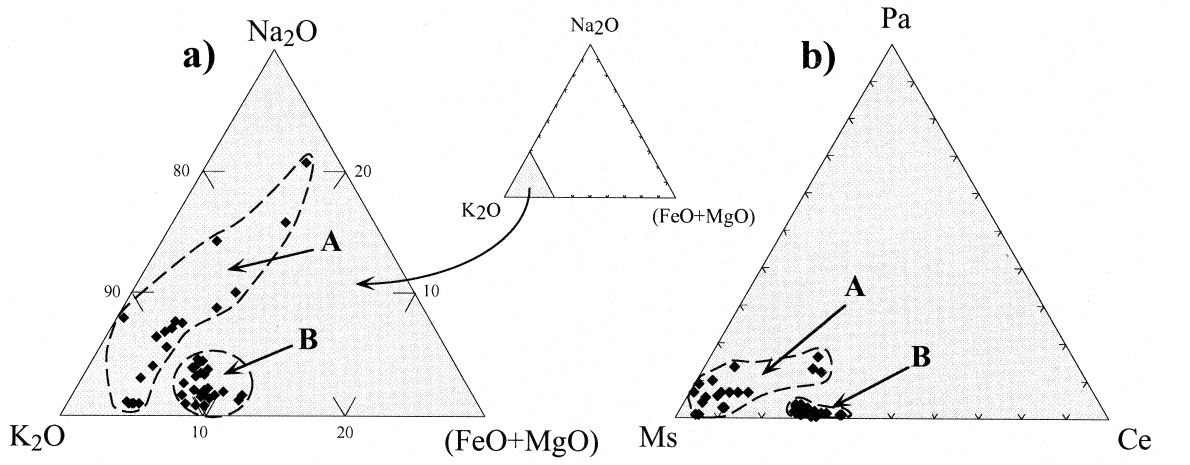

Fig. 7. Classification of the analysed muscovites from the studied rocks (**a**) according to the K_2O–Na_2O–(FeO + MgO) diagram, and (**b**) in terms of muscovite ($Ms = KAl_3Si_3O_{10}(OH)_2$), paragonite ($Pa = NaAl_3Si_3O_{10}(OH)_2$) and celadonite ($Ce = K(Mg,Fe)(Fe,Al)Si_4O_{10}(OH)_2$) end members. **A** = coarse-grained muscovites (large euhedral crystals) from Cueva de la Mora and Monte Romero massive ores (phengite content ≈0.50). **B** = fine-grained sericites from the hydrothermally altered footwall rocks at the ATE, San Miguel and Concepción stockworks (phengite content ≈0.80–1.15).

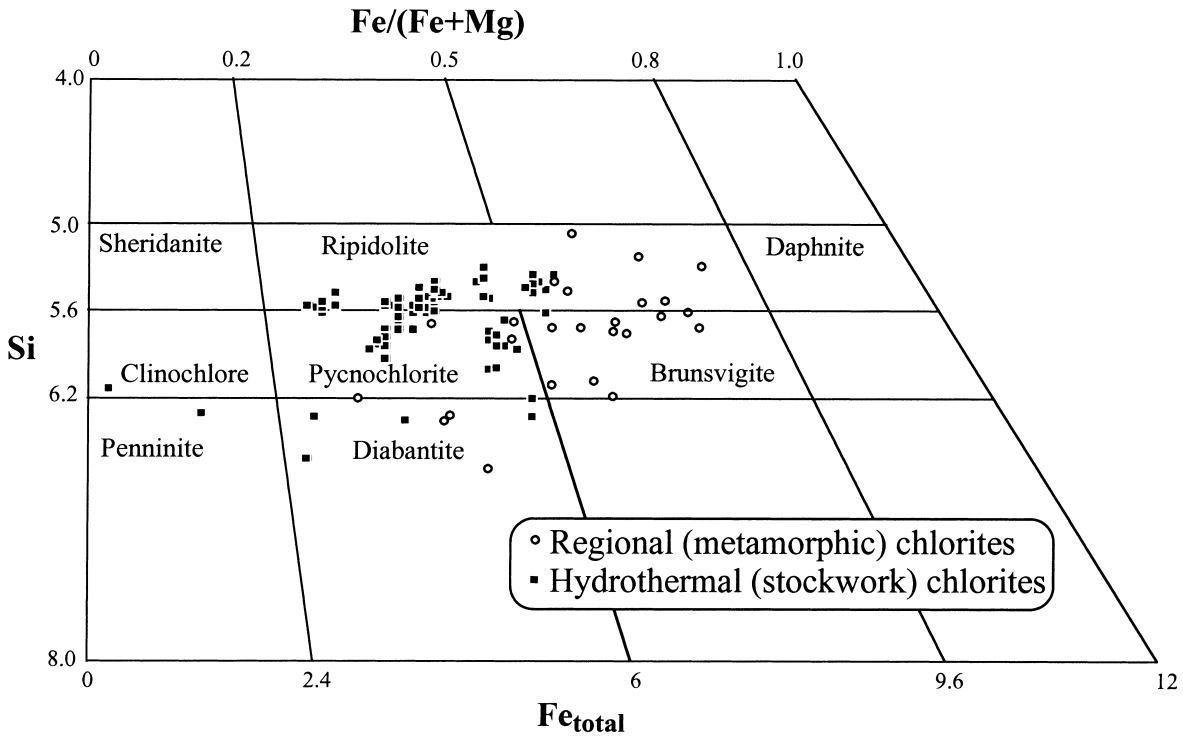

Fig. 8. Composition of the analysed chlorites from the hydrothermally altered footwall rocks in the studied deposits. For comparison purposes, regional (metamorphic) chlorites from distal unaltered sediments are also plotted (classification after Hey, 1954).

0.10–0.40 wt.% BaO, and no significant variation with distance from the immediate footwall to more external zones.

Chlorite is predominantly ripidolite to pycnochlorite in composition (Fig. 8). Its Fe/(Fe + Mg) ratio varies from values close to 0.30 (e.g., San Miguel) up to 0.70 (e.g., Concepción or Cueva de la Mora). Chlorite in the chloritic footwalls of the deposits has a notably different composition from that of regional chlorite, which has higher Fe/(Fe + Mg) values, and is mainly of brunsvigitic to Fe–ripidolitic composition. A similar feature is found in the La Zarza and Riotinto deposits (Strauss et al., 1981, and Leistel et al., 1994, respectively), where there is an increase in the Mg content from distal (regional) to inner (stockwork) chlorites, but is the opposite of that found in the Masa Valverde and Aznalcóllar deposits (Toscano et al., 1993; Almodóvar et al., 1998). However, there is no apparent increase in the Si/Al ratio with increasing distance from the stockworks, unlike that of chlorite in the Aznalcóllar footwall (Almodóvar et al., 1998). Fluorine content is highly variable (0.20–0.85 wt.%) with no relation to ore proximity, whereas the TiO_2, BaO and Cr_2O_3 contents are uniformly low, never exceeding 0.10 wt.%. Geothermometric calculations based on Al^{iv} site occupancy (Cathelineau, 1988) have yielded temperatures ranging from 220 to 380°C for chlorite crystallization in the central (chloritic) stockwork zones of the deposits (Fig. 9). These temperatures are slightly higher than those obtained for chlorites in more distal (sericitic) areas of the stockworks and mas-

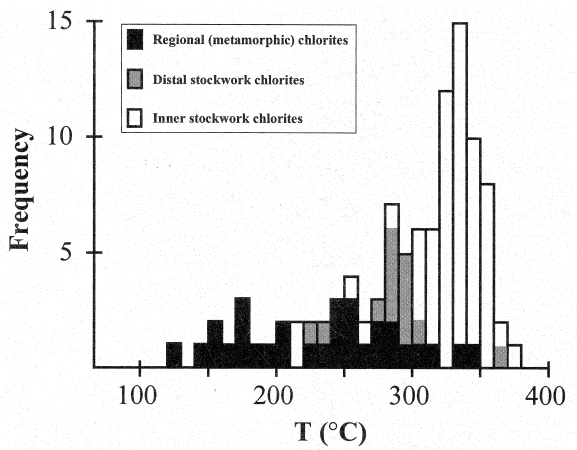

Fig. 9. Frequency histogram showing the range of the estimated crystallization temperatures for the analysed chlorites. Data calculated after the Al^{iv} cation site occupancy method of Cathelineau (1988).

sive ores, and show a fairly narrow range (shifted to higher temperatures) when compared with that of regional (metamorphic) chlorites.

Carbonate is common both in the footwall volcanics and the massive mineralization. It is usually present as a void filling, showing coarse-grained and poikiloblastic textures. Calcite and ankerite are the most frequent carbonate minerals, although dolomite may also be present (e.g., Aguas Teñidas Este; Fig. 10). The Fe/(Fe+Mg) ratio is, in most cases, similar to that observed in the chlorites, ranging from 0.30 to 0.70. The Mn content is important in some ankerites, with the rhodochrosite proportion ranging between 3 and 7%.

4.3.1. Fluid inclusion microthermometry

About 450 primary two-phase liquid-rich inclusions have been studied on 20 samples of stockwork vein quartz from the Aguas Teñidas Este, San Miguel and San Telmo deposits (Sánchez-España et al., in prep.). Fluid inclusions range from 2 to 18 μm in size, and are polygonal to tabular in shape. They are usually isolated and commonly lie within the growth planes of the quartz crystals, which often show a clear growth zoning. Most fluid inclusions have yielded homogenization temperatures ranging between 130 and 280°C, and salinities of 6–14 wt.% NaCl eq. (Fig. 11). Exceptionally, a few fluid inclusions found in milky vein quartz from the ATE stockwork have yielded lower temperatures (82–110°C) and higher salinities (16–24 wt.% NaCl eq.). These unusually saline fluid inclusions are scarce, and could have resulted from local boiling of the mineralizing fluid. The measured ore-related fluid inclusions are clearly different in composition from those of metamorphic origin found in quartz samples collected from Late Hercynian veins of the San Miguel, Soloviejo and Riotinto areas. Metamorphic fluid inclusions have a similar homogenization temperature range (120–270°C) to those of the hydrothermal fluid inclusions, but have notably lower salinities (averaging 4 wt.% NaCl eq.). Ore-related fluid inclusions have salinities higher than seawater (≈3.5 wt.% NaCl eq.), than those reported for most Kuroko-type deposits (≈3.5–7 wt.% NaCl eq.; Pisutha-Arnold and Ohmoto, 1983) and than many present-day hydrothermal systems (≈4 wt.% NaCl eq.). In short, the data point to a highly evolved seawater as the most probable source for the hydrothermal ore-forming fluid, and also imply an intense interaction of seawater with the underlying volcanic and sedimentary rocks. Such interaction would have resulted in acidification and chemical modification of seawater, and would have promoted the mineralogical and chemical modifications observed in the altered rocks.

These data show fluid inclusion temperatures similar to slightly lower than those determined in some studies centered on other IPB deposits such as Riotinto and Aznalcóllar (Nehlig et al., 1998, and Toscano et al., 1997, respectively), but the salinities shown in this study are overall much higher than those of other IPB deposits, of 1–12 wt.% NaCl eq. Both parameters increase at Aznalcóllar from the periphery to the stockwork and massive sulphide zones (Toscano et al., 1997).

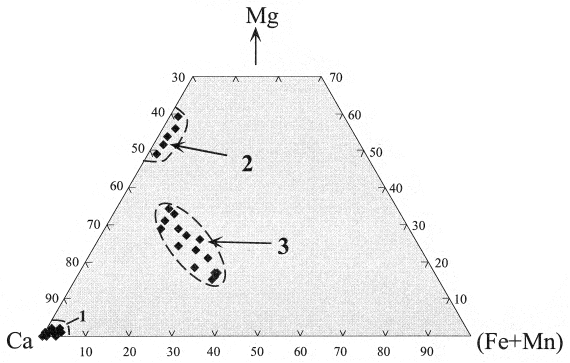

Fig. 10. Classification of the analysed carbonates from some of the studied deposits in the Mg–Ca–(Fe+Mn) diagram: (1) calcite and (2) dolomite from the ATE orebody; (3) ankerites from the ATE and Cueva de la Mora deposits.

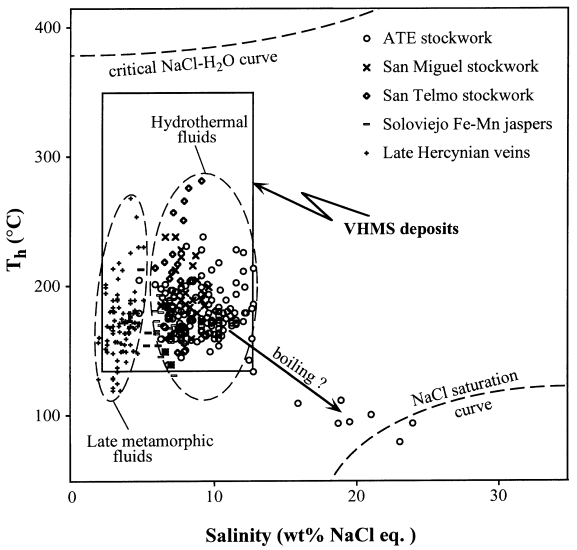

Fig. 11. T_h vs salinity diagram for the measured fluid inclusions from quartz–chlorite–pyrite stockwork veins of the ATE, San Miguel and San Telmo massive sulphide deposits. For comparison, data from the Soloviejo Fe–Mn-rich jasper mineralization, and from some Late Hercynian quartz veins of the San Miguel, Soloviejo and Riotinto deposits, have also been plotted.

Table 2
Bulk rock compositions of the least-altered, sericitized and chloritized felsic volcanic rocks, selected for the mass balance calculations[a]

	Least-altered rocks							Sericitized rocks										Chloritized rocks										
Sample No.	JB24	JB25	JB33	JB34	JB35	JB36	**Median**	CM4	CM8	CO4/1	CO18	COg5	CM23	AE5/18	AE5/24	AE5/25	AE5/23	**Median**	AE15.10	AE56.23	AE15.12	CO97stk	CO5	SMri	SMrvol	SM.stk	SM4	ST.stk	**Median**
SiO_2	79.66	76.34	82.82	82.38	78.35	71.96	**79.01**	72.89	65.59	74.05	73.70	76.29	62.16	78.07	72.09	66.16	71.77	**72.49**	57.34	73.40	69.07	45.03	69.62	71.88	53.29	62.52	67.55	61.28	**65.04**
TiO_2	0.08	0.12	0.07	0.06	0.08	0.10	**0.08**	0.33	0.27	0.16	0.17	0.10	0.28	0.14	0.16	0.19	0.15	**0.16**	0.08	0.09	0.13	0.17	0.09	0.13	0.21	0.19	0.16	0.15	**0.14**
Al_2O_3	11.78	12.10	9.21	8.65	12.27	14.87	**11.94**	16.71	18.02	13.30	12.30	11.43	17.23	11.21	12.16	17.01	12.82	**13.06**	5.48	6.96	9.78	12.80	7.28	7.72	9.73	9.91	8.63	8.84	**8.74**
Fe_2O_3t	0.34	0.73	0.78	0.64	1.15	1.27	**0.76**	0.44	2.95	1.89	3.28	1.98	3.49	1.31	2.52	2.94	1.99	**2.25**	22.53	8.06	9.84	23.11	13.56	8.43	17.34	16.61	10.17	13.87	**13.71**
MnO	0.00	0.00	0.01	0.04	0.01	0.02	**0.01**	0.01	0.04	0.03	0.07	0.02	0.20	0.04	0.02	0.02	0.02	**0.03**	0.10	0.08	0.02	0.19	0.11	0.07	0.09	0.20	0.09	0.11	**0.09**
MgO	0.26	0.13	0.25	0.20	1.07	0.82	**0.25**	0.74	5.97	3.02	2.57	1.34	4.88	2.82	5.09	5.85	3.78	**3.40**	4.34	6.49	1.55	9.27	4.82	8.06	9.69	5.14	8.50	10.16	**7.28**
CaO	0.05	0.06	0.03	0.04	0.08	0.11	**0.05**	0.01	0.31	0.13	0.53	0.00	0.98	0.31	0.74	0.65	1.58	**0.42**	0.38	0.00	0.00	0.01	0.00	0.00	0.00	0.02	0.02	0.00	**0.00**
Na_2O	2.39	2.36	0.99	1.09	0.71	3.76	**1.72**	0.43	2.52	0.82	2.14	0.33	0.75	1.30	0.79	1.95	0.91	**0.86**	0.05	0.00	0.09	0.00	0.02	0.00	0.00	0.10	0.02	0.00	**0.01**
K_2O	5.40	7.75	5.18	4.93	6.19	3.91	**5.29**	4.73	0.99	3.37	2.80	5.61	5.72	1.61	1.75	1.44	2.00	**2.40**	0.01	0.33	3.07	0.00	0.01	0.04	0.00	0.10	0.02	0.00	**0.01**
P_2O_5	0.01	0.01	0.01	0.01	0.01	0.01	**0.01**	0.02	0.02	0.02	0.01	0.01	0.05	0.01	0.01	0.01	0.01	**0.01**	0.00	0.00	0.01	0.00	0.01	0.00	0.00	0.02	0.00	0.00	**0.00**
LOI	0.25	0.35	0.47	1.17	0.25	2.23	**0.41**	3.50	3.30	3.65	3.10	2.41	47.26	3.15	4.03	4.75	4.70	**3.58**	10.26	4.83	7.00	8.45	4.84	5.02	10.02	5.51	6.13	6.35	**6.24**
ΣOx	100.22	99.96	99.81	99.21	100.17	99.05	**99.88**	99.81	99.97	100.42	100.67	99.53	99.98	99.96	99.37	100.96	99.73	**99.96**	100.55	100.25	100.56	99.03	100.35	101.35	100.38	100.31	101.29	100.76	**100.46**
As	1	8	2	4	2	2	**2**	73	109	3	2	17	32	12	4	2	10	**11**	104	73	46	65	65	2	37	115	6	7	**56**
Ba	251	316	526	513	537	285	**415**	2442	418	449	284	669	616	309	373	690	365	**434**	613	94	1043	60	70	251	164	64	168	101	**133**
Co	41	60	66	55	33	17	**48**	35	10	11	22	28	16	52	31	16	18	**20**	303	34	138	90	108	35	62	31	30	43	**52**
Cr	14	19	0	11	32	10	**13**	12	17	18	29	28	4	20	19	15	20	**19**	19	38	30	18	52	16	20	6	18	27	**20**
Cs	11	2	0	12	9	24	**10**	3	0	2	0	2	42	2	5	0	6	**2**	0	0	17	0	0	0	0	0	11	0	**0**
Cu	1	4	15	20	0	0	**2**	37	3	0	3	33	18	0	0	0	17	**3**	5924	5	6	34	134	0	15	101	40	154	**37**
F	6	0	226	42	1075	1319	**134**	1056	2852	435	896	650	2655	782	2118	1980	1682	**1369**	1753	2231	1459	1628	1316	1798	1744	738	1798	2281	**1748**
Nb	7	7	8	14	9	11	**8**	7	24	5	21	12	18	13	5	11	9	**11**	15	6	16	26	16	9	40	8	20	17	**16**
Ni	2	5	2	3	3	2	**3**	1	9	3	3	1	14	3	5	6	4	**3**	1	2	1	1	1	2	1	1	0	1	**1**
Pb	8	15	9	4	5	4	**6**	1538	16	2	11	12	13	16	5	3	7	**11**	20	20	7	136	172	5	9	8	8	5	**9**
Rb	82	111	143	137	171	156	**140**	151	31	114	97	129	301	46	72	59	81	**89**	12	17	120	9	5	4	9	10	4	6	**9**
S	350	4872	698	989	67	239	**524**	1851	654	838	0	968	112	2835	0	111	663	**659**	71021	10974	45048	5587	13632	3444	19137	2457	6547	5367	**8761**
Sn	0	0	0	0	0	0	**0**	6	0	0	0	1	2	0	0	0	0	**0**	41	4	56	16	47	10	14	2	10	11	**13**
Sr	68	57	27	26	28	55	**41**	39	139	16	71	33	101	81	46	87	57	**64**	25	9	18	10	13	9	12	12	10	8	**11**
V	11	13	11	12	13	13	**12**	30	15	15	11	15	24	12	27	22	32	**18**	9	10	14	17	15	11	14	24	14	13	**14**
Y	44	46	44	43	43	50	**44**	14	135	46	61	53	76	68	40	50	72	**57**	35	48	64	42	34	45	57	39	47	50	**46**
Zn	13	9	23	21	26	28	**22**	76	356	36	116	29	125	99	87	86	73	**86**	61	260	16	339	294	135	113	56	254	74	**124**
Zr	154	187	81	82	91	114	**103**	316	363	154	342	119	355	179	198	259	204	**232**	111	131	196	166	98	136	200	115	148	146	**141**
La	35	39	45	41	30	33	**37**	24	66	25	48	41	47	46	36	38	52	**43**	11	23	28	13	22	23	25	29	26	18	**23**
Ga	13	9	10	9	14	18	**12**	51	26	16	21	18	26	15	17	25	18	**20**	18	11	17	43	20	11	22	18	17	18	**18**
Th	4	4	7	6	5	10	**6**	6	12	9	8	5	11	5	8	10	10	**8**	29	7	15	16	7	9	14	8	8	13	**11**
Nd	36	32	44	47	37	37	**37**	63	61	35	43	44	45	47	48	66	54	**47**	22	18	43	21	15	25	22	20	21	18	**21**
Ce	90	79	115	123	95	94	**94**	173	162	88	109	115	117	122	125	180	142	**124**	44	34	109	37	24	56	44	38	43	32	**40**
Co/Ni	24	11	27	20	11	9	**15**	54	1	4	7	32	1	19	7	3	5	**6**	226	17	103	67	81	23	46	30	92	32	**57**
Zr/TiO_2	0.19	0.15	0.12	0.13	0.12	0.11	**0.13**	0.10	0.14	0.10	0.20	0.12	0.13	0.13	0.13	0.14	0.13	**0.14**	0.14	0.14	0.15	0.10	0.11	0.10	0.09	0.06	0.09	0.10	**0.10**
Nb/Y	0.15	0.15	0.18	0.34	0.22	0.22	**0.19**	0.48	0.18	0.12	0.35	0.23	0.23	0.20	0.14	0.22	0.12	**0.20**	0.43	0.12	0.25	0.62	0.46	0.20	0.69	0.20	0.42	0.34	**0.34**
AIm	0.07	0.08	0.14	0.12	0.24	0.21	**0.13**	0.19	0.72	0.54	0.54	0.36	0.56	0.59	0.75	0.72	0.66	**0.63**	1.00	0.98	0.88	1.00	1.00	1.00	1.00	0.99	1.00	1.00	**1.00**
AIt	0.03	0.04	0.05	0.06	0.04	0.06	**0.04**	0.07	0.24	0.06	0.21	0.09	0.15	0.20	0.16	0.09	0.17	**0.15**	0.90	0.74	0.20	0.85	0.86	0.36	0.49	0.76	0.63	0.68	**0.60**

[a] Major oxides in weight percent, trace elements in ppm; LOI, Loss on Ignition; AIm and AIt, Alteration Indices for major and trace elements, respectively; CO, Concepción; SM, San Miguel; AE, Aguas Teñidas Este; ST, San Telmo; CM, Cueva de la Mora.

4.4. Bulk rock geochemistry: composition of least-altered and altered rocks

Whole rock chemical analyses of some selected least- to strongly-altered rocks are given in Table 2. Although 176 samples were petrographically studied and analysed, only the ones given in Table 2 ($n = 26$) are considered to be representative of their respective groups (least-altered, sericitized and chloritized rocks) and, consequently, these only were used for the geochemical and mass balance calculations. The remaining samples ($n = 150$) included extremely altered volcanic rocks of uncertain origin, very fine-grained tuffites of mixed volcano-sedimentary derivation, intermediate to basic rocks (e.g., tholeiitic basalts), and other rocks not directly related to mineralization.

The analytical data confirm the rhyolitic character of the least-altered rocks (Table 2; Fig. 12). Notwithstanding their high SiO_2 and K_2O contents, their relatively low proportions of Fe_2O_3, CaO and Na_2O, as well as the heterogeneity in the SiO_2, Al_2O_3, Fe and Mg contents, are indicative of moderate regional silicification and sericitization affecting these rocks. The data support the idea that, even in areas distal to the ore deposits, unaltered volcanic rocks in the IPB are very rare, and some regional alteration is always present. However, least-altered rocks show no sign of sulphide mineralization and, consequently, have very low concentrations of chalcophile metals (e.g., Zn, Cu, Pb, Sn) and S.

Most of the analysed elements appear to have been mobilized during alteration, as their concentrations vary corresponding to the different types of alteration. Compared with the composition of least-altered rocks, the most striking differences are marked decreases in SiO_2, K_2O and Na_2O, and a related increase in the Fe_2O_3, MgO, MnO and LOI contents (Fig. 13(A)–(F)). Most major components appear to have been mobile, and only TiO_2 and P_2O_5 seem to have been unaffected by alteration. Aluminium (as Al_2O_3) shows strong percentage differences between the chloritized and least-altered rocks, although the apparent variations are mainly due to modal increases in other phases (such as Fe_2O_3, MgO or LOI), and may not be directly related to alteration; this is discussed below.

There are major compositional differences for many trace elements (e.g., Zn, Cu, As and Sn, as well as S, Sr, Rb and Ba), both within and between alteration types (Table 2). On the other hand, some elements like Zr, Nb, Y, Th, V, Ga, Ni and some LREE (La, Ce and Nd) are quite similar between the studied samples, being in most cases moderate to highly correlated ($r \approx 0.75$–0.83). However, the Th, Ga and Ni contents are frequently close to or below the detection limits of the analytical technique and should be taken with caution.

In agreement with the observations made by Strauss et al. (1981) and Almodóvar et al. (1998) in the La Zarza and Aznalcóllar deposits, respectively, a marked variation in the Co/Ni ratio has been observed in the altered rocks of the studied deposits (Table 2). However, this study does not confirm the direct relation suggested by these authors between the Co/Ni ratio and increasing alteration. This may be due to the highly felsic character of the sampled rocks, which always show very low Ni concentrations. Higher Co/Ni ratios (Table 2) reflect an increase in the Co content in highly mineralized samples. The high correlations observed between Co and S ($r = 0.97$), and between Co and As ($r = 0.91$), together with results of the microprobe analysis of the sulphides present in the altered rocks, indicate that Co is mainly introduced in mineral phases such as arsenopyrite (which shows Co contents up to 1%), glaucodot or cobaltite.

4.5. Use of median values for the mass change estimations

The choice of the precursor to any altered rock is critical when establishing chemical changes due to alteration as the results will largely depend on the initial composition of the chosen protolith. Due to destruction of the original texture and mineralogy of the altered rocks in the studied deposits, and also to abrupt lateral changes of the volcanic facies in the field, it is usually difficult to ascertain whether a given rock is the altered equivalent of another one some distance from the alteration zone. In this study, using a

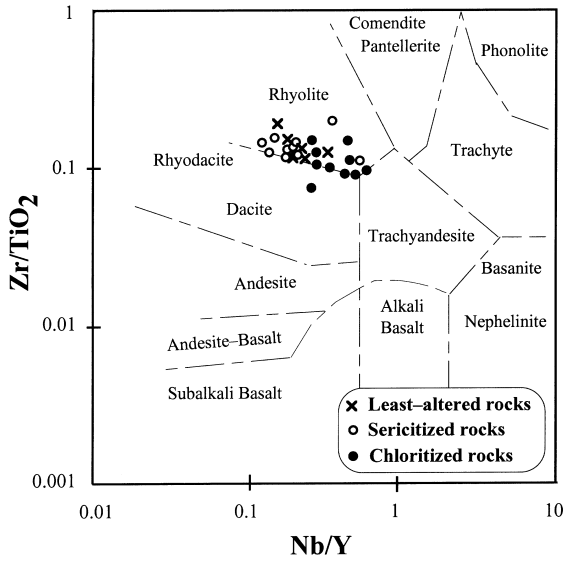

Fig. 12. Classification of the analysed volcanic rocks in the Zr/TiO_2 vs Nb/Y diagram (after Winchester and Floyd, 1978).

combination of geological, petrographic and geochemical criteria, rhyolitic volcanic rock of composition, similar to the analyses shown in Table 2, has been assumed as the least-altered precursor of the altered rocks.

In order to quantitatively estimate the mass changes accounted in the volcanic rocks due to hydrothermal alteration, chemical comparisons have been made among the respective medians of the (i) least-altered, (ii) sericitized, and (iii) chloritized rock groups

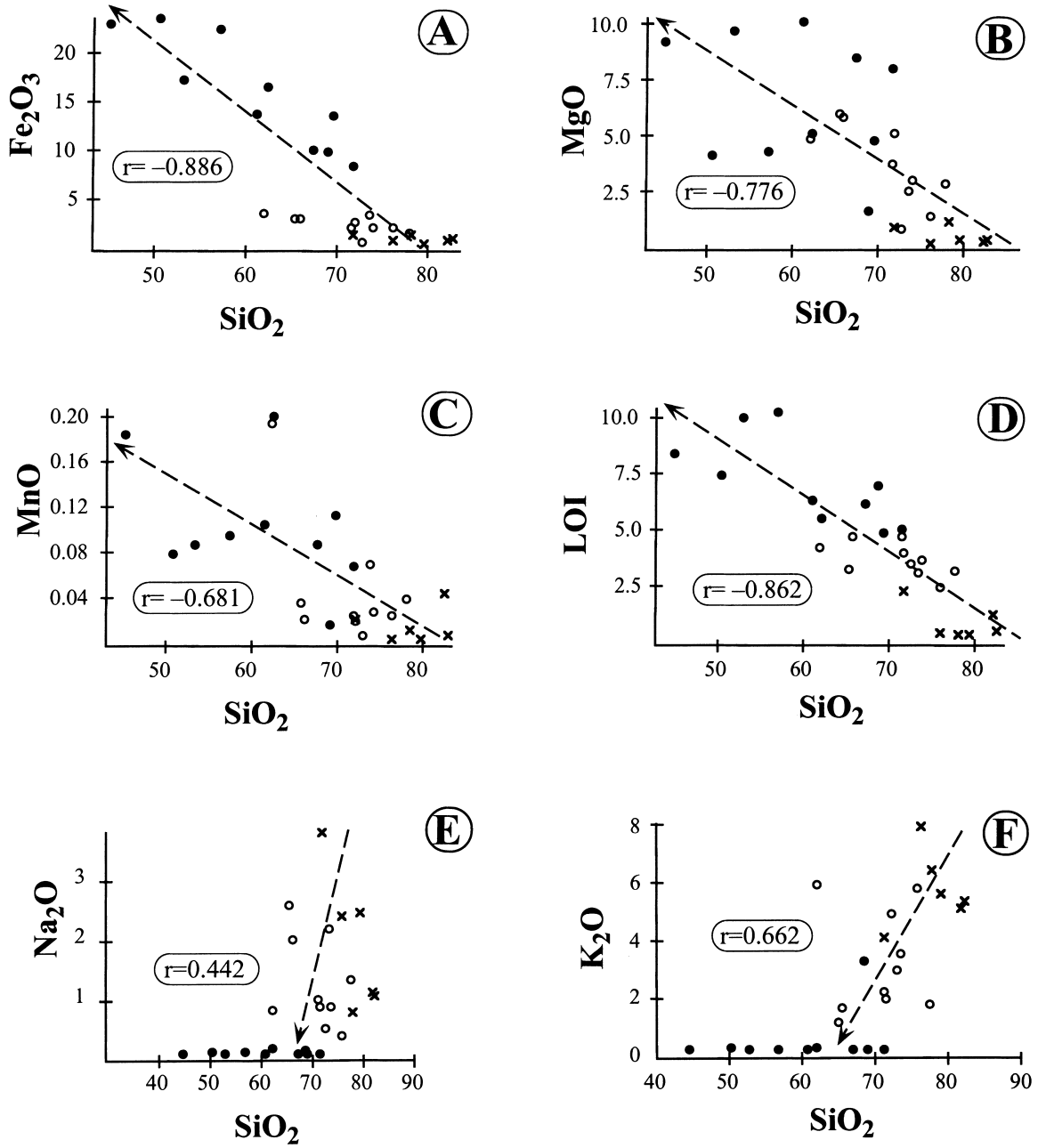

Fig. 13. (A) Fe_2O_3, (B) MgO, (C) MnO, (D) LOI, (E) Na_2O and (F) K_2O vs SiO_2 binary plots, for the rocks analysed. Dashed regression arrows indicate the alteration trend. Pearson's Product correlation coefficients (r) have been calculated using all samples (n = 26), with the significance value <0.01 in all cases. Symbols: *X-shaped symbols* — least-altered rocks; *empty circles* — sericitized rocks; *black circles* — chloritized rocks.

(Table 2). The use of this statistical parameter instead of the chemical analyses of specific least-altered, sericitized or chloritized samples, minimizes the error introduced by the heterogeneity observed within the three rock groups. In any case, the median values are similar to the chemical analyses corresponding to the most representative samples of each group, selected on the basis of petrographic observations. This is exemplified by the analytical similarities of samples JB24, CO4 and ST.stk (respectively, the most representative of the least-altered, sericitized and chloritized rocks) with the median values for their appropriate groups (Table 2).

4.6. Definition of the immobile elements and mass balance calculations

Direct comparisons between chemical analyses of least-altered and altered rock, using oxide weight percentages of the major constituents, are not useful, as they do not take into account volume changes that accompany mass transfer. A reference frame is needed to convert variations in chemical composition into units of mass transfer (Gresens, 1967). Grant (1986) modified the equations given by Gresens (1967) to develop his "Isocon method" for the calculation of absolute and relative mass or volume changes, associated with alteration. This method requires selection of immobile elements to define an isocon with which to compare mass gains or losses of the "mobile" elements. An isocon of slope 1 represents a net mass change of zero, with elements plotting below or above the isocon, representing mass loss or mass gain, respectively. Gresens (1967) suggested the use of Al, Ti, Zr, Y, Nb and Sc to monitor volume changes. These elements have been considered as relatively immobile in most hydrothermal systems by many authors (Winchester and Floyd, 1978; Finlow-Bates and Stumpfl, 1981; Lesher et al., 1986; MacLean and Kranidiotis, 1987; Elliot-Meadows and Appleyard, 1991; Gemmell and Large, 1992; MacLean and Barrett, 1993). Conversely, they have been shown to be mobile in other situations (Gibson et al., 1983; Naschwitz and Van Moort, 1991; Rubin et al., 1993; Huston and Cozens, 1994; Bjerkgärd and Bjørlykke, 1996; Tiwary and Deb, 1997). In the context of the IPB massive sulphide deposits, some authors have proposed that the elements Al, Zr, Ti, Nb, Y, P and REE are immobile during moderate alteration (Munhá, 1983; Thiéblemont et al., 1998). Others have reported variable mobility of some of these elements during alteration, as for example in Aznalcóllar (with mobilization of Zr, Y, Hf, REE and Al; Almodóvar et al., 1998), Salgadinho (Ti and Al mobility; Plimer and Carvalho, 1982) and other deposits (Pascual et al., 1997).

In the present study, both the constant Zr/TiO_2 and Nb/Y ratios between least-altered and altered samples (Table 2; Fig. 12), as well as the relatively good correlation coefficients obtained for some immobile-compatible and immobile-incompatible element pairs, suggest that these elements have behaved as essentially-immobile during alteration. Correlation coefficients are high in the cases of TiO_2–Zr and Al_2O_3–Zr ($r = 0.83$ and $r = 0.82$, respectively), and moderate to high for other component pairs such as TiO_2–Al_2O_3 ($r = 0.80$), Nd–Al_2O_3 ($r = 0.79$), Al_2O_3–Ce ($r = 0.78$) and Y–La ($r = 0.79$). Moreover, when plotting compatible-incompatible and compatible-compatible component pairs such as TiO_2–Zr and TiO_2–Al_2O_3 (Fig. 14(A) and (B)), a single alteration line is identified, which indicates a single precursor system and a chemically homogeneous volcanic unit (MacLean and Barrett, 1993; Barrett and MacLean, 1994). Fig. 14(A) and (B) also permits recognition of mass changes along the alteration line with respect to the average least-altered precursor, so that a widespread mass loss during sericitization and a net mass gain during chloritization can be easily recognized. Consequently, taking into account these observations, the HFS elements Al, Ti, Zr, Y, Nb and LREE (La, Ce and Nd) were used to monitor mass transfer in the isocon calculations. Their use to define the isocon has made it possible to establish net mass changes for the altered rocks. Such changes for each alteration type (sericitization and chloritization) with respect to the selected least-altered equivalent are shown in the isocon plots of Fig. 15, and are summarized in Table 3. Absolute gains and losses of major oxides and S are illustrated in Fig. 16.

In both Figs. 15(A) and (B), Nb, Y, Zr, P and the LREE (La, Ce and Nd; not shown in figures) define a straight line which is considered to be the best fit isocon and confirms the assumption that these elements have been effectively inert during all varieties of alteration. Similarly, Al and Ti plot very close to the isocons in both diagrams and, although there has been some migration, their mobility has not been significant and they can be considered as largely immobile elements (suggested in Fig. 14(B)).

Widespread addition of Fe, Mg and LOI, with corresponding loss of alkalis, appears to account for the major chemical changes in mobile components in the more altered rocks. Thus, sericitized rocks have gained considerable amounts of Mg, Fe and LOI (mostly H_2O, but also some CO_2), as well as some Ca and Mn (Figs. 15(A) and 16; Table 3). On the other hand, these rocks have lost important amounts of Si, K and Na. The isocon slope of 1.03 ± 0.07 gives a slight net mass loss of about 3% for these rocks. Chloritized samples exhibit a more intense alteration, showing a strong enrichment in Fe, Mg, water (LOI), and minor quantities of Si, Mn and S, with marked depletion in K, Na and, to a lesser degree, Ca and Rb (Figs. 15(B)

and 16; Table 3). These rocks also show a moderate gain in metals such as Zn, Cu, As and Sn. The relative mass change (given by an isocon slope of 0.78 ± 0.07) implies in this case a net mass gain of about 28%.

Composition-volume diagrams showing relative and absolute mobilities of major oxides (Gresens, 1967; Potdevin, 1993; Fig. 17) confirm the chemical changes displayed in the isocon plots. They also support the idea that chloritization involved greater element mobility and net mass change than sericitic alteration. In addition, calculated rock densities of least-altered (d = 2.76 gr/cm^3, n = 8), sericitized (d = 2.77 gr/cm^3, n = 8), and chloritized (d = 2.90–3.72 gr/cm^3, average of 3.59 gr/cm^3, n = 10) samples point to a net mass gain of about 30% for the chloritic rocks during alteration, in agreement with the isocon estimations.

4.7. Alteration Indices

Alteration Indices (AI), first proposed by Ishikawa et al. (1976), help to estimate the degree of alteration of felsic volcanic rocks hosting VHMS deposits. These

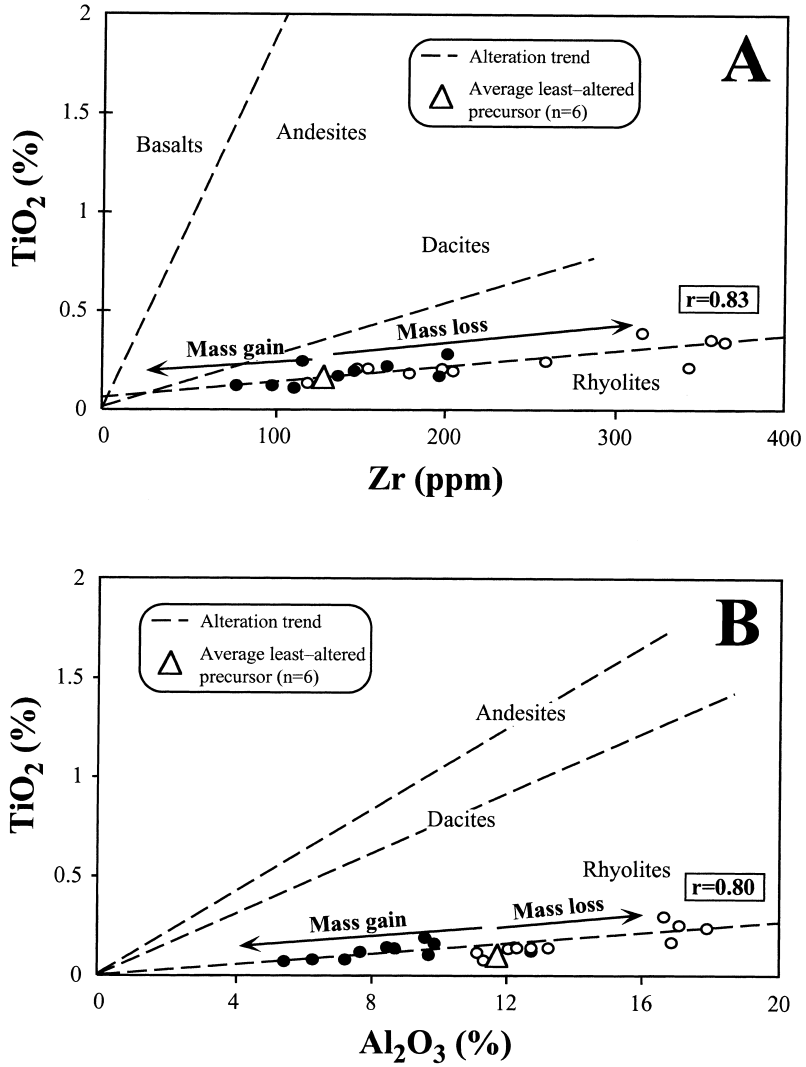

Fig. 14. (A) TiO_2–Zr, and (B) TiO_2–Al_2O_3 binary plots for the altered samples and average least-altered precursor. In both diagrams, a single alteration trend is obtained, thus indicating an initially homogeneous rhyolite unit (single precursor system). Sericitic samples show a widespread mass loss with respect to the least-altered precursor, whereas a net mass gain can be recognized in chloritic rocks. The Pearson's Product correlation coefficients (r) have been calculated using all the altered samples (n = 20), with the significance value <0.01 in both cases. Reference dashed lines and volcanic rock fields after MacLean and Barrett (1993). Symbols: *empty circles* — sericitized rocks; *black circles* — chloritized rocks.

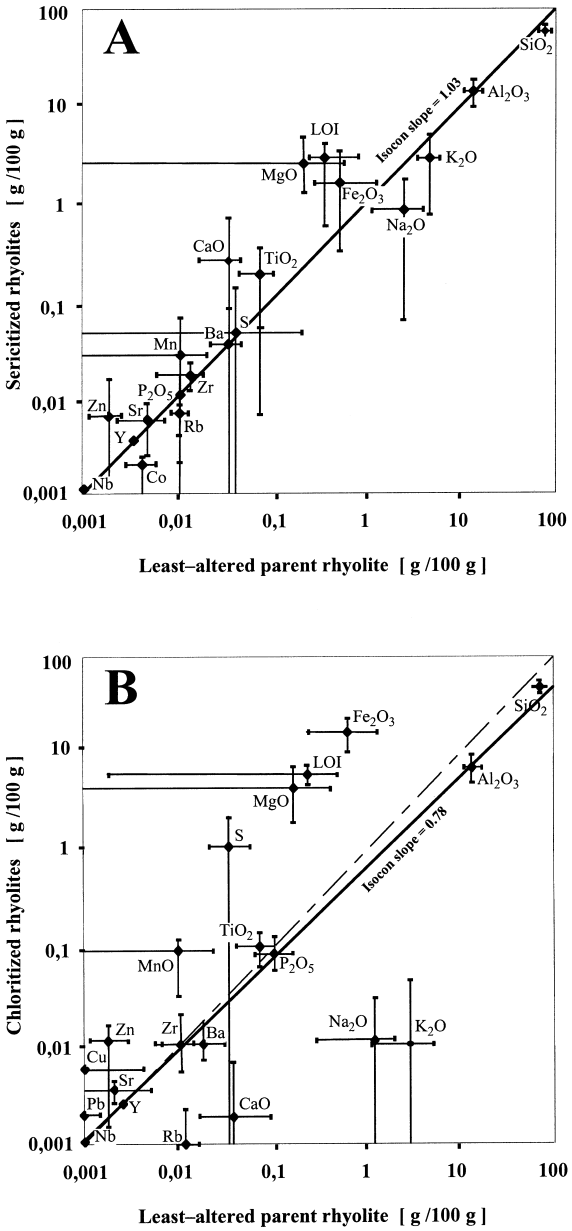

Fig. 15. Isocon diagrams for (A) sericitized, and (B) chloritized volcanic rocks. In these plots, relative mass changes of the major elements in the altered rocks with respect to their least-altered equivalent (as well as their respective standard deviations in the isocon calculations) are shown. Bold solid lines are the obtained best fit isocons, whose slope gives the net mass change in the altered rocks; the dashed line on (B) represents a reference isocon with ideal slope of one (mass change = zero); elements plotting below or above the isocons are depleted or enriched, respectively. For simplification, only major oxides and some trace elements have been plotted.

Table 3
Calculated mass changes (in g/100 g and %) for major oxides and S, accounted during sericitization and chloritization of the studied volcanic rocks, compared with the composition of the least-altered rocks

	Sericitization		Chloritization	
	Mass change (g/100 g)	Mass change (%)	Mass change (g/100 g)	Mass change (%)
SiO_2	−8.51	−10.8	2.25	2.9
Al_2O_3	0.76	6.4	−1.02	−8.5
TiO_2	0.07	87.9	0.01	100
Fe_2O_3	1.43	187.9	16.42	2153.7
MgO	3.07	1222.5	8.87	3538
MnO	0.02	191.7	0.10	1024.4
CaO	0.36	716.8	−0.05	−100
Na_2O	−0.91	−51.4	−1.71	−99.3
K_2O	−2.97	−55.9	−5.30	−99.8
P_2O_5	0.00	−2.8	0.09	118.6
LOI	3.08	749.1	7.41	1801.4
S	0.01	22.3	1.05	1988.8

authors proposed the equation $AI = [(MgO + K_2O)/(MgO + Na_2O + K_2O + CaO)]^*100$, although it is now suggested that any index relating enriched and depleted elements can be equally useful in the estimation of the alteration degree (Häussinger et al., 1993). Häussinger et al. (1993) calculated AI for the major (AI_{major}), and trace (AI_{trace}) elements separately, to improve the recognition of hydrothermal alteration. The AI_{major} versus AI_{trace} diagrams can be particularly helpful as they are sensitive to chemical variation related to hydrothermal alteration (Häussinger et al., 1993).

Considering the chemical tendencies observed in the analysed rocks (Tables 2 and 3; Figs. 13–17), and taking into account the above cited petrographic and mineralogical observations, the authors have used the following indices for the hydrothermally altered rocks:

$$AI_{major} = (Fe_2O_3t + MgO + MnO)/(Fe_2O_3t + MgO + MnO + Na_2O + K_2O)$$

$$AI_{trace} = (Zn + Cu + As + Sn)/(Zn + Cu + As + Sn + Sr + Ba + Rb)$$

The AI_{major} index (which creates values between 0 and 1) is very low (ranging between 0.07 and 0.24) in the least-altered rocks (Table 2). On the other hand, it is close to 1 in the more intensely chloritized samples, with sericitized rocks showing intermediate values.

When these values are plotted in an AI_{major} versus AI_{trace} diagram (Fig. 18), the distinction between the least-altered, sericitized and chloritized samples is clear, and helps to discriminate the degree of alteration of the host rocks. Thus, plots such as these can be effective and inexpensive tools in mine-scale exploration (especially when they are accompanied with petrographic studies), as they give additional information from drill-core or underground samples. However, use of this type of diagram should be restricted to massive sulphide districts linked to felsic volcanism (such as the IPB), since the cited diagrams become less useful when more basic host rocks (which would give higher AI_{major} values, even when least-altered) are involved.

5. Discussion and conclusions

5.1. Validity of the obtained results

Chemical changes during hydrothermal alteration are subject to several factors that could quantitatively vary and so introduce significant error in the calculated mass changes. The main variables, that substantially determine the results obtained by the isocon method, are: (i) the selected samples and their respective analyses, which may *or may not* be the most suitable examples of least-altered and altered volcanic rocks at each deposit; (ii) the choice of immobile elements for defining the isocon; and (iii) the assumption that alteration took place at constant volume.

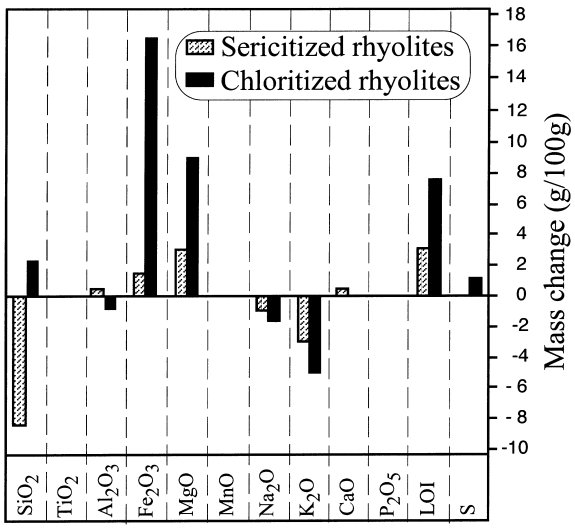

Fig. 16. Mass balance diagrams showing the calculated mass changes (in g/100 g) of major oxides and S in the hydrothermally altered rocks.

However, the results obtained are consistent with field observations, and the petrography and mineral chemistry of the rocks, and agree with observations reported by previous workers in other VHMS deposits worldwide (Gemmell and Large, 1992; Huston, 1993; MacLean and Barrett, 1993; Lentz and Goodfellow, 1993, 1996).

5.2. Behavior of the HFS elements

The observed immobility of the HFS elements is in agreement with previous studies on hydrothermal alteration of volcanic rocks of many VHMS districts (MacLean and Barrett, 1993, and references therein). On the other hand, the ubiquitous presence of tiny rutile and zircon crystals (directly related with hydrothermal phases such as chlorite, quartz or sericite) in the volcanic rocks and in the massive ores, is strong evidence for the local mobility of Ti and Zr during alteration, as noted in other IPB deposits (Pascual et al., 1997; Almodóvar et al., 1998). However, this mobility may have been on the micro (thin section) scale, and be related to local dissolution of Ti and Zr-bearing phases (such as magnetite and biotite, respectively), which are present in the least-altered rocks. Concentration or dilution of these elements is therefore probably a consequence of mass addition or mass reduction, by removal of other mobile components (e.g., Fe_2O_3, MgO, SiO_2, etc.), rather than a product of macro scale mobilization. This is corroborated by the lack of significant scatter shown in the Zr/TiO_2 versus Nb/Y diagram (Fig. 12), on which the majority of samples (both least-altered and altered) plot within a narrow range in the rhyolite field. This observation confirms the general validity of using these ratios in petrogenetic discussions. However, they should be taken with caution, if analysed rocks show local abundance of zircon and/or rutile of evident hydrothermal origin.

A noticeable decrease in the Al content of the chloritized rocks is apparent in some of the studied rocks. For most samples this is due to microveins composed of quartz and sulphide. However, some samples have no sign of microfracturing or vein filling, so that Al depletion in their bulk compositions could be the result of metasomatic exchange between the rocks and the hydrothermal fluids. Aluminium has been traditionally used to monitor and normalize mass changes in altered host rocks of the IPB massive sulphides (Léistel et al., 1994; Bobrowicz, 1995) and elsewhere (e.g., Lentz and Goodfellow, 1996). However, this element has been shown to be variably mobile during hydrothermal alteration in certain massive sulphide deposits (Plimer and Carvalho, 1982; Gibson et al., 1983; Naschwitz and Van Moort, 1991; Bjerkgärd and Bjørlykke, 1996; Tiwary and Deb, 1997), as well as in the vein gold

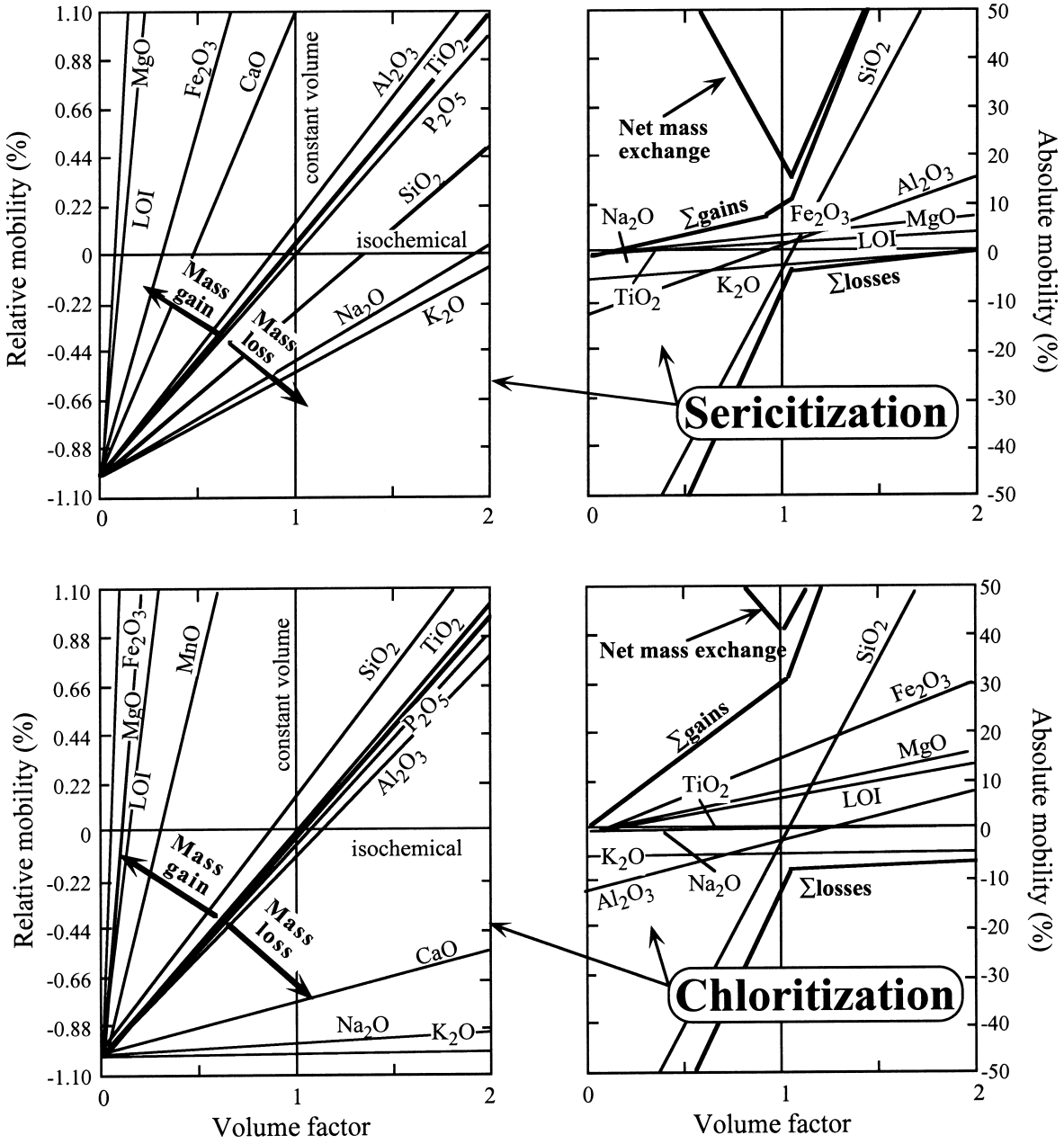

Fig. 17. Composition-volume diagrams showing relative and absolute mobilities of major oxides, during sericitization and chloritization of the analysed rhyolitic volcanics — after Gresens (1967) and Potdevin (1993). Note that, for a volume factor of one (i.e., constant volume), less mobile oxides (TiO_2, P_2O_5 and Al_2O_3) show an almost isochemical behavior (both relative and absolute mobility approach zero). On the other hand, mobile elements display trends which lay above (mass gain) or below (mass loss) those of the immobile elements. Calculations have been made with the "Gresens '92" Pascal program (Potdevin, 1993), taking into account the respective rock densities of least-altered, sericitic and chloritic rocks.

deposits of central Victoria in Australia (Gao and Kwak, 1997), the epithermal precious metal mineralization in the active geothermal system at northern Lesbos, Greece (Kontis et al., 1994), and in acid-sulphate epithermal systems (White and Hedenquist, 1998). In most cases this Al mobility has not been satisfactorily explained. In the context of the Iberian massive sulphide deposits, the dissolution and consequent migration of Al (in the form of Al^{3+} or $Al(OH)^{2+}$) could have been favoured by the severe physico-chemical conditions prevailing during the waxing stage of the ore-forming hydrothermal systems. In such an environment of high temperature, salinity and water/rock ratio, and, with a large proportion of chemical species such as HCl, H_2S or HF, Al mobilization would be thermodynamically feasible, taking place during the hydrolysis and pseudomorphic replacement of the feldspar and white mica by chlorite, late quartz and/or sulphide.

5.3. Alteration mechanism

According to models describing the geochemistry and mechanisms of hydrothermal alteration associated with massive sulphide deposits (Sangster, 1972; Solomon, 1976; Franklin et al., 1981; Lydon, 1988b, 1996; Large, 1977, 1992; Ohmoto, 1996), the chemical and mineralogical changes observed in the footwall rocks of such deposits can be explained as the result of several metasomatic processes. These involve hydration, cation exchange, dissolution, precipitation and redox reactions, and take place during the ascending circulation of hot modified seawater, through the feeder pathways of these deposits. During the lifetime of a convective cell, seawater is progressively modified as it descends in the upper crust and reaches hotter volcanic rocks. Such a system is open and dynamic, with fresh cold seawater continuously supplied on the periphery of the system, and continuous removal of the hot and modified ore-bearing fluid at the discharge area of a sulphide occurrence (Ohmoto, 1996). Consequently, as seawater progressively heats and gains metals, H_2S and CO_2, reactions between this ore-forming fluid and wall rocks occur in response to the changing physico-chemical conditions such as temperature, fluid pressure, O and S fugacities, pH or water/rock ratios (Pisutha-Arnold and Ohmoto, 1983; Large, 1992; Ohmoto, 1996; Lydon, 1996).

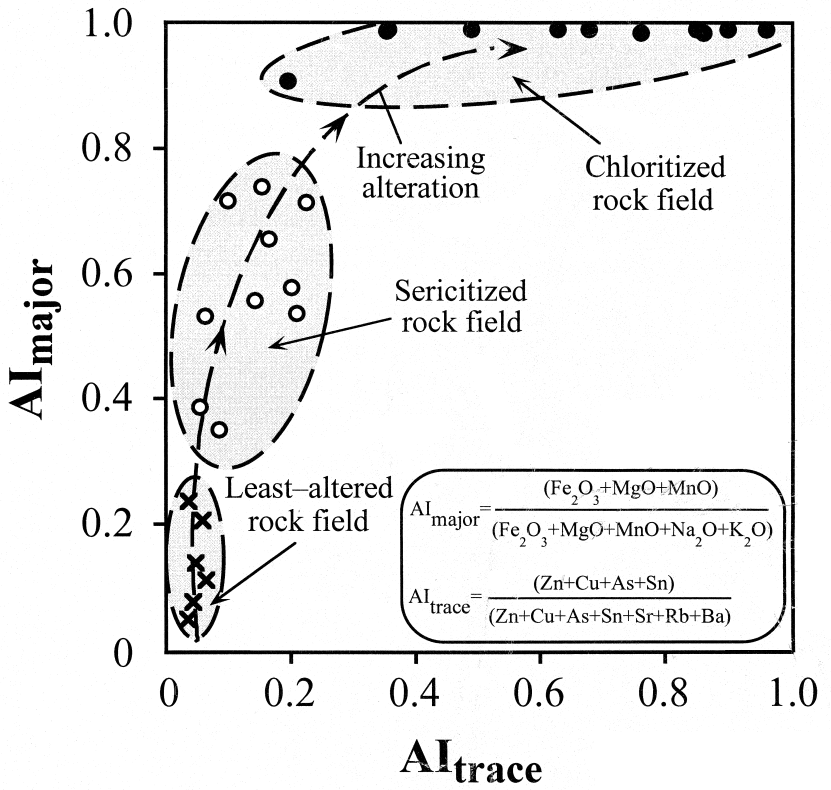

Fig. 18. AI_{major} vs AI_{trace} diagram showing the characteristic fields of the least-altered, sericitized and chloritized volcanic rocks (adapted from Häussinger et al., 1993).

The footwall rocks of the deposits of this study appear to have undergone several stages of alteration as temperature and water/rock ratios have increased. Sericitized rocks are best considered as an intermediate stage (rather than an independent type) of alteration between unaltered (or *weakly* altered) volcanics, and the most chloritized samples.

The following is proposed as an alteration history of the rocks during hydrothermal and mineralizing activities:

1. At an early stage, moderate temperature (150–250°C) and acidic (pH ≈ 4–5) ore-bearing fluid (circulating along the feeder pathways) reacted with unconsolidated and highly porous volcanic tuffs just below the seafloor, as well as with connate fluids. Primary minerals and volcanic glass of the host rocks acted as natural buffers for the chemically reactive fluid. Dissolution of feldspar (K-feldspar and albite phenocrysts, and also fine-grained crystals in the groundmass) occurred, with formation of fine-grained sericite and quartz, according to reactions of the type:

$$\underset{\text{K-feldspar}}{3KAlSi_3O_8} + 2H^+ \Longrightarrow \underset{\text{Muscovite}}{KAl_3Si_3O_{10}(OH)_2} + \underset{\text{Quartz}}{6SiO_2} + 2K^+$$

and

$$\underset{\text{Albite}}{3NaAlSi_3O_8} + K^+ + 2H^+ \Longrightarrow \underset{\text{Muscovite}}{KAl_3Si_3O_{10}(OH)_2} + \underset{\text{Quartz}}{6SiO_2} + 3Na^+$$

During this stage, some chlorite, pyrite and sphalerite would have also precipitated. These changes would have resulted in moderate K, Na and Si depletion, and slight gains in Fe, Mg and water.

2. In a later stage, a more evolved, hotter (300–350°C) and more acidic (pH ≤ 4) fluid, was responsible for intense alteration of the primary minerals. Water/rock ratios, H_2S activity and metal content in the hydrothermal fluid, were considerably higher than those in the previous stage, as would be the rate of cation exchange between rock and fluid, resulting in mobilization of most elements. All residual feldspar from the early stage, as well as previously formed sericite and quartz, was almost totally transformed to ripidolitic chlorite. A suggested reaction for such transformations is of the type:

$$\text{Muscovite} + 3Fe^{+2} + 4.5Mg^{+2} + 1.5\text{Quartz} + 12H_2O \Longrightarrow 1.5\text{Ripidolite} + K^+ + 14H^+$$

Precipitation of abundant pyrite and some chalcopyrite occurred during this stage. The chemical reflection of these changes resulted in a marked K and Na depletion, and a strong enrichment in Fe, Mg, H_2O, Si and S, with minor addition of metals such as Zn, Cu, As and Sn.

3. At some localities, continuation of stage (2) for an extended period produced further chemical and mineralogical transformations, leading to extremely chloritic rocks such as those found in some deposits (e.g., Aguas Teñidas Este or Cueva de la Mora), where the original rock fabric is completely obliterated and no sign of the primary minerals can be observed. An increase in the amount of CO_2 dissolved in the fluids was probably responsible for the local precipitation of Fe-rich carbonates (e.g., in the uppermost part of the Aguas Teñidas Este footwall alteration, or at Cueva de la Mora).

In the waning stage of the hydrothermal activity, there was some crystallization of silica, mainly as vein filling, in the central parts of the stockworks. This late coarse-grained quartz (together with some euhedral pyrite) sealed open veins and pores developed during the previous stages.

Processes such as these resulted in alteration zones beneath the massive sulphides exhibiting the presently observed geometry and characteristics, in which the limits between the chloritic and sericitic haloes to the unaltered footwall rock represent the palaeo-isotherms of the hydrothermal plume, at the maximum temperature stage of the hydrothermal system.

As the systems developed and then waned, the hydrothermal fluids, on encountering cold and reducing seawater, precipitated first massive sulphides, then Fe- and Mn-jaspers onto the ocean floor.

5.4. General conclusions and outlook

In conclusion, the authors note that all the above-documented observations (including petrography, mineral chemistry and mass balance calculations, and reported S isotope and fluid inclusion data) support the hypothesis of a continuous interaction of the volcanic rocks with an evolving and thermally increasing ore-bearing fluid, which would have been continuously venting through the volcanic pile. This hydrothermal fluid transferred abundant cations (Fe^{2+}, Mg^{2+}, Mn^+, Zn^+, Cu^+), anions ($S^=$, Cl^-) and volatiles (H_2O, CO_2) to, whilst leaching significant amounts of Na^+, K^+ and Si^{4+} from, the parent rock. Only a few elements such as Al, Ti, Zr, Nb, Y, P and LREE appear to have remained essentially inert during alteration. An immediate reflection of this chemical exchange between fluid and rock is the change in the rock mineral assemblages, necessary for chemical re-equilibration. The most important mineral changes

have been the destruction of the original volcanic constituents (hydrolysis of feldspar and dissolution of quartz), with subsequent precipitation of phases such as sericite, chlorite and pyrite, which pseudomorphically replaced the primary minerals.

This work emphasizes the importance of geochemical studies of footwall rocks of the IPB VHMS deposits in unravelling the nature and characteristics of the hydrothermal systems responsible for ore generation in the IPB. It has also shown that such studies can be useful in exploration for massive sulphides within the IPB, as they can reveal the extent of intense zoned hydrothermal alteration often associated with stringer-type and/or massive mineralization.

Acknowledgements

This work has been possible thanks to the Department of Education, Universities and Research of the Basque Government, which financially supports Javier Sánchez-España. Basque Country University is also thanked for its financial support (project UPV 130.310-EB037/9). Dr Kerr Anderson from Navan Resources (Huelva) S.A., and Jose Antonio Castro from Minas de Rio Tinto S.A.L., are gratefully acknowledged for their kind attention and the facilities they provided, including the collection of drill-cores and access to the mines. We would also like to thank Philippe de Parseval for his help and technical support with the microprobe analysis at the Université Paul Sabatier in Toulouse. We greatly appreciate the extensive and critical comments made by Drs G. Ewers, R. Large and R. Davy on a previous version of this manuscript, which have considerably improved the quality of the paper.

References

Almodóvar, G.R., Sáez, R., Pons, J.M., Maestre, A., Toscano, M., Pascual, E., 1998. Geology and genesis of the Aznalcóllar massive sulphide deposits, Iberian Pyrite Belt, Spain. Miner. Dep. 33, 111–136.

Barrett, T.J., MacLean, W.H., 1994. Mass changes in hydrothermal alteration zones associated with VMS deposits of the Noranda area. Expl. Min. Geol. 3, 131–160.

Barriga, F.J.A.S., 1983. Hydrothermal metamorphism and ore genesis at Aljustrel, Portugal. Ph.D. thesis, University of Western Ontario, Canada.

Barriga, F.J.A.S., Fyfe, W.S., 1998. Multi-phase water-rhyolite interaction and ore fluid generation at Aljustrel, Portugal. Miner. Dep. 33, 188–207.

Baumgartner, L.P., Olsen, S.N., 1995. A least-squares approach to mass transport calculations using the Isocon method. Econ. Geol. 90, 1261–1270.

Bjerkgärd, T., Bjørlykke, A., 1996. Sulphide deposits in Folldal, Southern Trondheim region Caledonides, Norway, source of metals and wall–rock alterations related to host rocks. Econ. Geol. 91, 676–696.

Bobrowicz, G.L., 1995. Mineralogy, geochemistry and alteration as exploration guides at Aguas Teñidas Este, Pyrite Belt, Spain. Unpubl. Ph.D. thesis, University of Birmingham, UK.

Bonaño, A.S., Vázquez, F.C., Borrero, J.D., Ramos, T.N., 1984. Memoria explicativa de la Hoja Geológica 1:50.000 de El Cerro de Andévalo (No. 937). I.G.M.E.; 2ª serie, Madrid.

Boulter, C.A., 1993a. High level peperitic sills at Riotinto, Spain: implications for stratigraphy and mineralization. Trans. Inst. Min. Met. London 102, B30–B37.

Boulter, C.A., 1993b. Comparison of Rio Tinto, Spain: and Guaymas Basin: Gulf of California. An explanation of a supergiant massive sulphide deposits in an ancient sill-sediment complex. Geology 21, 801–804.

Bryndzia, L.T., Scot, S.D., Farr, J.E., 1983. Mineralogy, geochemistry and mineral chemistry of siliceous ore and altered footwall rocks in the Uwamuki 2 and 4 deposits, Kosaka mine, Hokuroku district, Japan. Econ. Geol. Monograph 5, 507–522.

Carvalho, D., Correia, H.A.C., Inverno, C.M.C., 1976. Livro guia das excursoes geologicas na Faixa Piritosa Iberica. Comun. Serv. Geol. Port. 60, 271–315.

Cathelineau, M., 1988. Cation site occupancy in chlorite and illites as a function of temperature. Clay Minerals 23, 471–485.

Elliot-Meadows, S., Appleyard, E.C., 1991. The alteration geochemistry and petrology of the Lar Lake Cu–Zn deposit, Lynn lake area, Manitoba, Canada. Econ. Geol. 86, 486–505.

Fernández, Alvarez G., 1974. Los yacimientos de sulfuros polimetálicos del SO Ibérico y sus métodos de prospección. Ph.D. thesis, University of Salamanca.

Fernández-Caliani, J.C., Mesa, J.M., Galán, E., 1994. Características del metamorfismo de grado bajo a muy bajo en la parte meridional de la Faja Pirítica (Zona Sur Portuguesa). Bol. Geol. Miner. 105 (2), 213–220.

Finlow-Bates, T., Stumpfl, E.F., 1981. The behaviour of so-called immobile elements in hydrothermally altered rocks associated with volcanogenic submarine-exhalative ore deposits. Mineral Dep. 16, 319–328.

Franklin, J.M., Sangster, D.F., Lydon, J.W., 1981. Volcanogenic massive sulphide deposits. Econ. Geol. 75th Anniv., 485–627.

Gao, Z.L., Kwak, T.A.P., 1997. The geochemistry of wall rock alteration in turbidite-hosted gold vein deposits, central Victoria, Australia. J. Geochem. Explor. 59, 259–274.

García, Palomero F., 1980. Carácteres geológicos y relaciones morfológicas y genéticas de las mineralizaciones del Anticlinal de Riotinto. Inst. Estud. Onubenses "Padre Marchena", Excma. Diput. Prov. de Huelva.

Gemmell, J.B., Large, R., 1992. Stringer system and alteration zones underlying the Hellyer volcanic-hosted massive sulphide deposit, Tasmania, Australia. Econ. Geol. 87, 620–649.

Gibson, H.L., Watkinson, D.H., Comba, C.D.A., 1983. Silicification, hydrothermal alteration in an Archean geothermal system within the Amulet Rhyolite Formation, Noranda, Quebec. Econ. Geol. 83, 954–971.

Goodfellow, W.D., Peter, J.M., 1994. Geochemistry of hydrothermally altered sediment, Middle Valley, northern Juan de Fuca Ridge. Proceedings of the ODP: Scientific Results 139, 207–289.

Grant, J.A., 1986. The isocon diagram — a simple solution to Gresen's equations for metasomatic alteration. Econ. Geol. 81, 1976–1982.

Gresens, R.L., 1967. Composition-volume relations of metasomatism. Chem. Geol. 2, 47–65.

Häussinger, H., Okrusch, M., Scheepers, D., 1993. Geochemistry of premetamorphic hydrothermal alteration of metasedimentary rocks associated with the Gorob massive sulphide prospect, Damara Orogen, Namibia. Econ. Geol. 88, 72–90.

Hey, M.H., 1954. A new review of the chlorites. Mineralog. Mag. 30, 277–292.

Huston, D.L., 1993. The effect of alteration and metamorphism on wall rocks to the Balcooma and Dry River South volcanic-hosted massive sulphide deposits, Queensland, Australia. J. Geochem. Explor. 48, 277–307.

Huston, D.L., Cozens, G.J., 1994. The geochemistry and alteration of the White Devil porphyry, implications to intrusion timing. Miner. Dep. 29, 275–287.

Ishikawa, Y., Sawaguchi, T., Iwaya, S., Horiuchi, M., 1976. Delineation of prospecting targets for Kuroko deposits based on modes of volcanism of underlying dacites and alteration haloes. Min. Geol. 26, 105–117.

Kontis, E., Kelepertsis, A.E., Skounakis, S., 1994. Geochemistry and alteration facies associated with epithermal precious metal mineralization in an active geothermal system, northern Lesbos, Greece. Mineral. Dep. 29, 430–433.

Large, R.R., 1977. Chemical evolution and zonation of massive sulphide deposits in volcanic terrains. Econ. Geol. 72, 549–572.

Large, R.R., 1992. Australian volcanic-hosted massive sulphide deposits, features, styles, and genetic models. Econ. Geol. 87, 471–510.

Lécolle, M., 1977. La ceinture sud-ibérique, un exemple de province à amas sulfurés volcano-sedimentaires. Thése, Univ. P. et M. Curie, Paris.

Leistel, J.M., Bonijoly, D., Braux, C., Freyssinet, Ph, Kosakevitch, A., Leca, X., Lescuyer, J.L., Marcoux, E., Milési, J.P., Piantone, P., Sobol, F., Tegyey, M., Thiéblemont, D., Viallefond, L., 1994. The massive sulphide deposits of the South Iberian Pyrite Province, geological setting and exploration criteria. Editions BRGM 234.

Leistel, J.M., Marcoux, E., Thiéblemont, D., Quesada, C., Sánchez, A., Almodóvar, G.R., Pascual, E., Sáez, R., 1998. The volcanic-hosted massive sulphide deposits of the Iberian Pyrite Belt. Mineral. Dep. 33, 2–30.

Lentz, D.R., Goodfellow, W.D., 1993. Petrology and mass-balance constraints on the origin of quartz–augen schist associated with the Brunswick massive sulfide deposits, Bathurst, New Brunswick. Can. Miner. 31, 877–903.

Lentz, D.R., Goodfellow, W.D., 1996. Intense silicification of footwall sedimentary rocks in the stockwork alteration zone beneath the Brunswick No. 12 massive sulphide deposit, Bathurst, New Brunswick. Can. J. Earth Sci. 33, 284–302.

Lesher, C.M., Goodwin, A.M., Campbell, I.H., Gorton, M.P., 1986. Trace elements of ore-associated and barren, felsic metavolcanic rocks in the Superior Province, Canada. Can. J. Earth Sci. 23, 222–241.

Lydon, J.W., 1988a. Volcanogenic massive sulphide deposits, Part 1, A descriptive model. Geoscience Canada Reprint Series 3. Ore Deposit Models, pp. 145–152.

Lydon, J.W., 1988b. Volcanogenic massive sulphide deposits, Part 2, Genetic models. Geoscience Canada Reprint Series 3. Ore Deposit Models, pp. 155–176.

Lydon, J.W., 1996. Characteristics of volcanogenic massive sulphide deposits, interpretations in terms of hydrothermal convection systems and magmatic hydrothermal systems. Bol. Geol. Min. 107 (3/4), 215–264.

MacLean, W.H., Barrett, T.J., 1993. Lithogeochemical techniques using immobile elements. J. Geochem. Expl. 48, 109–133.

MacLean, W.H., Kranidiotis, P., 1987. Immobile elements as monitors of mass transfer in hydrothermal alteration, Phelps Dodge massive sulphide deposit, Matagami, Quebec. Econ. Geol. 82, 951–962.

Mitjavilla, J., Martí, J., Soriano, C., 1997. Magmatic evolution and tectonic setting of the Iberian Pyrite Belt volcanism. J. Petrol. 38 (6), 727–755.

Mitsuno, C., Nakamura, T., Yamamoto, M., Kase, K., Oho, M., Suzuki, S., Thadeu, D., Carvalho, D., Arribas, A., 1988. Geological studies of the "Iberian Pyrite Belt" with special reference to its genetical correlation of the Yanahara ore deposits and others in the inner zone of southwest Japan. University of Okayama, Japan.

Munhá, J., 1979. Blue amphiboles, metamorphic regime and plate tectonic modeling in the Iberian Pyrite Belt. Contrib. Mineral. Petrol. 107, 153–162.

Munhá, J., 1983. Hercynian magmatism in the Iberian Pyrite Belt. The Carboniferous of Portugal. In: Sousa, M.J.L., Oliveira, J.T. (Eds.), Mem. Serv. Geol. Port., vol. 29, pp. 39–81.

Munhá, J., 1990. Metamorphic evolution of the South Portuguese/Pulo do Lobo Zone. In: Dallmeyer, R.D., Martínez, García E. (Eds.), Pre-mesozoic Geology of Iberia. Springer-Verlag, Berlin pp. 363–368.

Munhá, J., Kerrich, R., 1980. Sea water-basalt interaction in spillites from the Iberian Pyrite Belt. Contrib. Mineral. Petrol. 73, 191–200.

Naschwitz, W., Van Moort, J.C., 1991. Geochemistry of wall-rock alteration, Rosebery, Tasmania. Australia. Appl. Geochem. 6, 267–278.

Nehlig, P., Cassard, D., Marcoux, E., 1998. Geometry and genesis of feeder zones of massive sulphide deposits: constraints from the Rio Tinto ore deposit (Spain). Mineral. Dep. 33, 137–149.

Ohmoto, H., 1996. Formation of volcanogenic massive sulphide deposits: The Kuroko perspective. Ore Geol. Rev. 10, 135–177.

Pascual, E., Toscano, M., Almodóvar, G.R., Sáez, R., 1997. Zirconium mobility in footwall hydrothermal haloes in the Iberian Pyrite Belt: geochemical and textural evidences. In:

Barriga, F.J.A.S. (Ed.), Neves-Corvo SEG Field Conference, Lisbon, Portugal, 11–14 May 1997 Abstracts and program volume, 81.

Pinedo Vara I., 1963. Piritas de Huelva: Su historia, minería y aprovechamiento. Ed. Summa, Madrid.

Pisutha-Arnold, V., Ohmoto, H., 1983. Thermal history, chemical and isotopic compositions of the ore-forming fluids responsible for the Kuroko-massive sulphide deposits in the Hokuroku district of Japan. Econ. Geol. Monog. 5, 523–558.

Plimer, I.R., Carvalho, D., 1982. The geochemistry of hydrothermal alteration at the Salgadinho copper deposit, Portugal. Mineral. Dep. 17, 193–211.

Potdevin, J.L., 1993. Gresens 92: A simple Macintosh program of the Gresens method. Comp. and Geosci. 19, 1229–1238.

Ramírez, J., Navarro, D., 1982. Memoria explicativa de la Hoja geológica 1:50.000 de Nerva (No. 938). I.G.M.E., 2ª Seria.

Rodríguez, P., 1996. Aguas Teñidas Deposit, Faja Pirítica, Cu–Pb–Zn–Ag. In: Simposio Sulfuros polimetálicos de la Faja Pirítica Ibérica, Spain 21–23 February 1996.

Routhier, P., Aye, F., Boyer, C., Lécolle, M., Moliére, P., Picot, P., Roger, G., 1978. La Ceinture Sud-Ibérique a amás sulfurés dans sa partie espagnole médiane. Mem. BRGM 94.

Rubin, J.N., Henry, C.D., Price, J.G., 1993. The mobility of zirconium and other "immobile" elements during hydrothermal alteration. Chem. Geol. 110, 29–47.

Sáez, R., Almodóvar, G.R., Pascual, E., 1996. Geological constraints on massive sulphide genesis in the Iberian Pyrite Belt. Ore Geol. Rev. 11, 429–451.

Sánchez-España, F.J., Velasco, F., Yusta, I., 1997. Hydrothermal alteration geochemistry of some massive sulphide deposits at the Rio Tinto Syncline, Iberian Pyrite Belt, Spain, Papunen, , Mineral Deposits: Research and Exploration, Where do they Meet?, Proc. 4th Biennial SGA Meeting, Turku, Finland, pp. 375–378.

Sánchez-España, F.J., Velasco, F., 1999. Constraints on the Hercynian metamorphism at the NE Iberian Pyrite Belt: ore petrography and phyllosilicate crystallinity. In: Stanley, C.J. et al. (Eds.), Mineral Deposits: Process to Processing, Balkema, pp. 975–978.

Sangster, D.F., 1972. Precambrian volcanogenic massive sulphide deposits in Canada. A review. Can. Geol. Survey Paper, pp. 72–22.

Schermerhorn, L.J.G., 1970. The deposition of volcanics and pyrite in the Iberian Pyrite Belt. Mineral. Dep. 5, 273–279.

Schermerhorn, L.J.G., 1971. An outline stratigraphy of the Iberian Pyrite Belt. Bol. Geol. Min. 82, 239–268.

Schütz, W., Dulski, P., Germann, K., 1988. Geochemical features of magmatic evolution and ore deposition in the Pyrite Belt of Southern Spain. In: Freidrich, G.H., Herzig, P.M. (Eds.), Base Metal Sulfide Deposits. Springer-Verlag, Berlin, pp. 240–253.

Seyfried Jr, W.E., Berndt, M.E., Seewald, J.S., 1988. Hydrothermal alteration processes at mid-ocean ridges: constraints from diabase alteration experiments, hot spring fluids and composition of the ocean crust. Can. Min. 26, 787–804.

Silva, J.B., Oliveira, J.T., Riveiro, A., 1990. Structural outline of the South Portuguese Zone. In: Dallmeyer, R.D., Martínez, García E. (Eds.), Pre-Mesozoic Geology of Iberia. Springer-Verlag, Berlin, Heidelberg, New York pp. 348–362.

Soler, E., 1973. L'association spillites–quartz kératophyres du Sud-Ouest de la Péninsule Ibérique. Geol. Mijnbouw 52, 277–287.

Solomon, M., 1976. "Volcanic" massive sulphide deposits and their host rocks — a review and an explanation. In: Wolf, K.A. (Ed.), Handbook of Strata-Bound and Stratiform Ore Deposits, II, Regional Studies and Specific Deposits. Elsevier, Amsterdam pp. 21–50.

Strauss, C.K., Roger, G., Lécolle, M., Lopera, E., 1981. Geochemical and geological study of the volcano-sedimentary orebody of La Zarza, Huelva Province, Spain. Econ. Geol. 76, 1975–2000.

Thiéblemont, D., Marcoux, E., Teggey, M., Leistel, J.M., 1994. Genesis of the south-Iberian pyrite belt in a palaeoacretionary prism?: Petrological arguments. Bull. Soc. Géol. 165 (5), 407–423.

Thiéblemont, D., Pascual, E., Stein, G., 1998. Magmatism in the Iberian Pyrite Belt: petrological constraints on a metallogenic model. Mineral. Dep. 33, 98–110.

Tiwary, A., Deb, M., 1997. Geochemistry of hydrothermal alteration at the Deri massive sulphide deposit, Sirohi district, Rajasthan, NW India. J. Geochem. Explor. 59, 99–121.

Tornos, F., González-Clavijo, E., Spiro, B., 1998. The Fillón Norte orebody (Tharsis, Iberian Pyrite Belt): a proximal low-temperature shale-hosted massive sulphide in a thin-skinned tectonic belt. Mineral. Dep. 33, 150–169.

Toscano, M., Almodóvar, G.R., Sáez, R., Pascual, E., 1993. Hydrothermal alteration related to the "Masa Valverde" massive sulphide deposit, Iberian Pyrite Belt, Spain. In: Fenoll Hach-Ali P, Torres-Ruiz J, Gervilla F. (Eds.), Current research in geology applied to ore deposits, University of Granada, Spain, pp. 389–392.

Toscano, M., Almodóvar, G.R., Sáez, R., 1994. Variación composicional de las sericitas de alteración hidrotermal en sulfuros masivos: "Masa Valverde" (Huelva). Bol. Soc. Esp. Min. 17, 161–162.

Toscano, M., Sáez, R., Almodóvar, G.R., 1997. Hydrothermal fluid evolution during the genesis of the Aznalcóllar massive sulphides (Iberian Pyrite Belt): fluid inclusion evidences. Geogaceta 21, 211–214.

Urabe, T., Scott, S.D., 1983. Geology and footwall alteration of the South Bay massive sulphide deposit, northwestern Ontario, Canada. Can. J. Earth Sci. 20, 1862–1879.

Urabe, T., Scott, S.D., Hattori, K., 1983. A comparison of footwall–rock alteration and geothermal systems beneath some Japanese and Canadian volcanogenic massive sulphide deposits. In: Econ. Geol. Monograph 5. Society of Economic Geologists, El Paso, Texas, USA pp. 345–364.

Velasco, F., Sánchez-España, F.J., Boyce, A., Fallick, A., Sáez, R., Almodóvar, G.R., 1998. A new sulphur isotopic study of some IPB deposits: evidence of a textural control on the sulphur isotope composition. Mineral. Dep. 33 (8), 4–18.

White, N.C., Hedenquist, J.W., 1998. Epithermal environments and styles of mineralization. J. Geochem. Explor. 36, 445–474.

Winchester, J.A., Floyd, P.A., 1978. Geochemical discrimination of different magma series and their differentiation products using immobile elements. Chem. Geol. 20, 325–344.

Yusta, I., Velasco, F., Herrero, J.M., 1994. The determination of major oxide and 10 trace element concentrations in 58 geochemical reference samples by X-ray spectrometry (WD-FRX). Bol. Soc. Esp. Min. 17, 39–51.